Insertion of random spaces in time domain for frequency hopping sequences for RF systems

A thesis submitted to the Universidad EAFIT
in accordance with the requirements of the degree of
Doctor in Engineering in the School of Engineering

Augusto Carmona Valencia

School of Engineering
Universidad EAFIT
July 2020

Research Supervisor Dr. José Ignacio Marulanda Bernal
Head of Doctoral Program: Professor Francisco Javier Botero Herrera

Abstract

Improvements over the communications protocols are always a continuous research. Fast Frequency Hopping is an important method still in use and orthogonal codes used in SFH-CDMA are the special interest in several areas of technology. This research uses one coincident orthogonal code with restrictive adjacent spectral distance for the design of RF correlation detectors based on planar resonators arrays. Inclusion of uniform time delays sections between adjacent resonators is a well-known method to improve the MAI, at expenses of decrease the data rate and finally the bandwidth of protocol. Another strategy is selecting random delays between symbols in the way of adjacent peaks in cross correlation function vanishes, improving the dynamic range of asynchronous detector and accordingly the user number sharing the channel of communications.

Resumen

FFH es un método de acceso al canal con amplias aplicaciones pasadas y presentes, dentro de este método los códigos ortogonales usados en SFH-CDMA son de especial interés en amplias áreas de la tecnología. El presente trabajo implementa códigos ortogonales un coincidentes (1dOC) con restricciones en componentes espectrales adyacentes para el diseño de detectores auto correlacionados en RF que usan arreglos de sensores planos. La inclusión de retrasos temporales entre resonadores adyacentes es un método que permite disminuir la interferencia entre los usuarios (MAI), en contraposición a la disminución de la velocidad de transmisión y finalmente el ancho de banda del protocolo. La selección aleatoria de retrasos entre símbolos adyacentes reduce los máximos en la correlación cruzada, aumentando el rango dinámico del detector asíncrono y por ende el número de usuarios que comparten el canal de comunicaciones.

Declaration

This dissertation is submitted to Universidad EAFIT in accordance with the requirements for the degree of Doctor of Engineering in the School of Engineering. The research and thesis presented in this dissertation are entirely my own work and have not been submitted to any other university or higher education institution, or for any other academic award in this university. Where use has been made of other people's work, it has been fully acknowledged and referenced.

Augusto Carmona Valencia

July 2020

Certificate of Acceptance

Following a successful presentation and evaluation by the Research Evaluation Committee, this dissertation entitled INSERTION OF RANDOM SPACES IN TIME DOMAIN FOR FRQUENCY HOPPING SEQUENCES FOR RF SYSTEMS submitted by Augusto Carmona Valencia has been accepted.

Evaluation Committee

Juror 1	Signature: _____
Prof. Dr. Alcides Montoya Cañola	Date: September 28, 2020
Juror 2	Signature: _____
Dr. Ernesto Neira Camelo	Date: September 28, 2020
Juror 2	Signature: _____
Prof. Dr. Carlos Trujillo Anaya	Date: September 28, 2020

Thesis contributions

The current thesis presents the incidence of time delays inclusion for passive frequency synthesizer in SFH. Through measures in Laboratório de Sistemas Intergrades, IEAv, ITA, Sao Paulo, Brasil, it has developed a calibration method for the local laboratory, Universidad EAFIT, Medellín, Colombia.
Moreover, it was constructed a Ground Station system for Amateur bands used in CubeSats satellites from 2016-2017, using SDR and open Source elements.

During the development of this research work the following publications were developed:

A. Carmona, M. C. Carvalho, J. I. Marulanda and A. C. da Cunha Migliano, Análise de Simulações Eletromagnéticas em Linhas de Transmissão na faixa de micro-onda da Banda-X, Revista Diálogos Interdisciplinares, 2019, Vol. 8 issue 2 ISSN 2317-3793.

V. Toro-Betancur, A. Carmona V., and J. I. Marulanda, Signal detection and modulation classification for satellite communications, October 2020, ACM Singapore Chapter, ISBN 978-1-4503-7573-3

Participations in international events:

A. Carmona, M. C. Carvalho, J. I. Marulanda and A. C. da Cunha Migliano, Simulações Eletromagnéticas em microfitas com linhas ressoadoras na Banda – X por meio do método MDFDT, IX ENCIBRAC Encontro Científico, setembro 2019, Mogi das Cruzes, São Paolo, Brasil.

Acknowledges

I would like to thank to my thesis director, the knowledge, inspiration, and support, without this supply the final research would not have been possible; to Physics Laboratory Department for all the technical help and collaboration in models and characterization; to all the support of my family in the process. To IEAv, ITA and Professor Migliano, Chief of Laboratório Multiusuário de Sistemas Eletromagnéticos in San Jose dos Campos, SP, Brazil, his discussions and experience allow to me understand each topic of this research and clarify a little more the beautiful Electromagnetic Theory.

Thanks a lot to Colciencias – Colfuturo, with the 6172 Project Doctoral National Internships, all the financial support and incredible organization and optimization of resources. Thanks to that I could improve my skills in academy and human variables.

Contents

List of Figures

List of Tables

List of Abbreviations

AFH	Adaptative Frequency Hopping
BER	Bit Error Rate
DS-CDMA	Direct Sequence Code Division Multiple Access
DWDM	Dense Wavelength Division Multiplexing
EMC	Electromagnetic Computational
ESR	Electron Spin Resonance
FBG	Fiber Bragg Grating
FDTD	Finite Difference Time Domain
FH-SS	Frequency Hopping Spread Spectrum
ISM	Industrial, Scientific and Medical Band
MAI	Multiple Access Interference
MIC	Microwave Integrated Circuit
MKID	Microwave Kinetic Inductance Detectors
OC	Orthogonal Codes
OC1d	Orthogonal Codes one coincident with adjacent restriction
OCDMA	Optical Code Division Multiple Access
OST	Open Short Through
PTL	Planar Transmission Lines
QoS	Quality of Service
SFH-CDMA	Slow Frequency Code División Multiple Access
SIR	Signal to Interference Ratio
SOLT	Short, Open, Load and Thru Calibration method
SQUID	Superconducting Quantum Interference Device
TDR	Time Domain Reflectometry

Chapter I

Introduction

Generation of efficient orthogonal sequences is a problem to guarantee QoS in communication protocols in a tradeoff of increasing the complexity of computing generation. One coincident case [1] with restriction in adjacent spectral distance is optimum in several ways, especially for cross correlation method of detection, exploiting the asynchronous access with inexpensive hardware architecture complexity. Chip time in DS-CDMA is equally distributed; in particular, SFH-CDMA is composed by dwell and dead times that prevent the switching hardware requirements. The insertion of this time slots improves significantly the MAI [2] and avoid collision between similar frequencies. In this research, time delay distribution between adjacent symbols is time randomly, decreasing cross correlation side lobes, improving dynamic range, and increasing indirectly the number of users sharing the channel.

1.1. Orthogonal Codes

The introduction and study of sequences used in FH-SS corresponds to several studies that cover from 70's until now [2]. The election of DS-CDMA for the third generation of cellular by 3GPP increased the search for bipolar efficient orthogonal sequences, improving the number of users, easily to implement in software and hardware, with low probability of eavesdropping, low cross correlation and high auto correlation. Among the most used sequences are the pseudo noise sequences (PN) [3], maximal length sequences, Gold and Kasami sequences and so on [4]. However, the one coincident case [1] is an over performance case, but with limitation of available codes, as the result of the number of user to shared media. However, high autocorrelation and low side lobes of cross correlation make these codes a reference case to test the time distribution.

Within a family $\mathcal{F}$ of υ frequencies, the main idea to implement is to find $\mathcal{M}$ FH orthogonal

sequences with optimal Hamming cross and auto correlation function [5]. Maximize the number of codes increase the users number but decrease lightly the orthogonal properties. The definitions of aperiodic Hamming function [6] improves this requirement. However, the probability of collision between adjacent frequencies is an open problem to solve. AFH is a modern alternative to share the communication channel in an intelligent way [7], using the advances in digital technology.

One of the most attractive characteristics of hopping frequency-based systems is their high resistant method against Jamming and eavesdropping. In fact, the first applications were in military scenarios [8][9]. The codes used in Fathallah [10] research are not the optimal for the optical application; Bin [1] and orthogonal cases uses this type of codes to prevent collisions in FH-CDMA, mainly due to Doppler effect and avoid MAI, but the optical frequency synthesizer allows to introduce passive variables over the structure avoiding digital requirements like synchronization and high speed processing. The continuous search for optimization of codes for another set of applications arises of mathematical and engineering application in telecommunications and cryptography technology. Linear complexity represents [11] a parameter to optimize and the number of users is a hot topic to increase the network capacity.

The cross-correlation coder-encoder has experimented many changes on timeline passing to digital era. For the fiber optic communication case, the fiber Bragg gratings (FBG) established a lot of attention in sensing methods and potential application for photonics technology [12][13]. Recently, resonant structures in planar microwave lines has received a lot of attention provided by quantum circuits to induce selective photons number over SQUID section [14], opening a prolific research area in ESR [15], quantum information [16], particle detection [17], magnetic field orientation [18] among others.

1.2. Noncoherent Detection

Although the main application of orthogonal codes is in CDMA communication field (including cryptography) [2], it could be extrapolated to FBG network sensing [19]and in SQUID multiplexers or techniques where the arrays of frequencies required individual selection with a posterior uncovered behavior inside a high random noise. The S-band as a testing

part is a very attractive case for different facts. The high interference in certain spectral regions like 2.40 GHz (ISM) allows to include possible testing values in a crowded communication band, with special consideration in cognitive radio scenarios for future swarm of satellite communications [20].

To test the performance of the insertion of random slot times, the present research takes the BER as comparative element. For different communication protocols, performance manager applying standards for BER are: DS1 is limited by 6.5×10^{-7}, DS3 with 2.2×10^{-8} and finally, for the case OC3 is around 6.4×10^{-9}. Telcordia, for example uses 10^{-6} to generate minor alarms over the communication and major alarms over 10^{-3} [21]. Although, for some clients this last value represents lost communication. So, values of 10^{-6} are a good tread off for RF links while for optical is 10^{-9}.

Frequency synthesizers used in OCDMA with FBG [10], based in cross correlation incoherent detection, decreases the complexity and improve the response using only passive elements. Competition for time and power in modern FH are the hardest and bottleneck implementation case [22][15]. Inclusion of passive elements could reduce these problems, solving without increasing the complexity of the system in all. However, the high Q on the FBG improves the selectivity of the system for OCDMA. Implementation in RF synthesizer using planar microwave technology is limited for the material characteristics. All the implementations and testing part in this research use RO4350B® [23] and the symbols are fixed in S band (ISM). Considering the high traffic in this spectrum range is a good concept to test the system against high noise floor.

The contribution presented in this document is the improvement performance in SFH-CDMA using random time delays between adjacent frequency symbols over correlation detectors. Dynamic range is increased in a factor of two; reduction of sidelobes of cross correlation decreases the probability of false detection. Finally, inclusion of blank spaces, equivalent to spectral encoding in the optical case OCDMA [24], is not the most efficient method in comparison with a correct election of adjacent time/space delays. The method presented here does not increase directly the number of users, but reduces adjacent cross correlation peaks and noise floor, decreasing the MAI.

1.3. Thesis Overview

For the development of this research, the subsequent organization was followed; first chapter presents the main characteristics of orthogonal codes, used as symbol generators. The one oincidence with constraint adjacent spectral distance is the main example to use through the text using mainly two families of codes; $\mathcal{H} = (29,12,0,1)$ and $\mathcal{H} = (13,4,0,1)$. This was done due to disposal of previous scientific articles to compare proper simulation with reported data. One characteristic of this families founded is the possibility to classify and find better options between them, getting generalization over the previous results. The chapter ends with the inclusion of random time delays displaying the spreading of sidelobes into the initial blank spaces and comparing uniform distribution with the randomly spaces using one coincident family generators.

The second chapter introduces the microstrip method of design and fabrication. Static approximation is exhibited and used for numerical simulations. Linear resonators with the proper techniques of characterization, within the circuit model and computer simulation, match according with the experimental method within a margin of 0.5% of error. The testing experimental cases was used to compare computational response on time and frequency domain used in future design of synthesizers and for the confidence of the simulations. Microstrip technology is a very well standard techniques with high scale of reproducibly [25]. However, fabrication technique is an important issue to take in account using local technology. The chapter ends with the inclusion of time delays and their characterization using TDR technique. An analysis of physical delays in time domain is an important part over the final synthesizer design.

Next chapter explains the methods of simulation and characterization used throughout study. FDTD [26][27] is the numerical method used and XFdtd® 7.3 is the software selected for simulations. This part of the document presents the main microwave structures used to final design as well as some testing experimental results to compare with simulation results. The use of FDTD requires a high computational power. However, the results are very close to experimental cases. The big limitation here is that these structures are resonant devices. The chapter ends with Network Analysis, additional to the description of TDR method, which was used for previously discussed time delay measures.

Section 5 presents the frequency synthesizer design, testing with the family $\mathcal{H} = (13,4,0,1)$, comparing the uniform spacing case and randomness. The design proposed here only evaluates the cross-correlation detection using one coincident case and delays between adjacent symbols. Response of resonator to room temperature is certainly different in quality factor against FBG, but the essence of problem is the same. MAI reduction is achieved with similar margin presented before in section 2.5 and dynamic range improvement is in order of twice using random distribution of delays against uniform distributions.

Finally, it is presented some general conclusions about the random approach in RF synthesizer, some developments and future studies generated by the random insertion of time delays and bibliography references that support the research.

Chapter II

Orthogonal Codes in SFH-CDMA

The present chapter shows some generalities about OCs, mathematical foundations, and the measures of performance against MAI using BER variable. The main purpose is to introduce the factors and types of codes used in different spread spectrum communications systems, applicable in fiber optics and RF case, i.e. pseudo random sequences used in Bluetooth®, radar systems identification and sonar devices. Although the BER is the main objective function to improve, the definitions of Auto and Cross Correlation Hamming functions will be used to compare different type of codes.

There are many ways to get orthogonal codes for 1D case; OOC (optical orthogonal codes), PC (prime codes), QCC (quadratic codes) and so on. The main interest for the present case is the OOC, which represent the codes with the best performance against the cross-correlation function and multiuser interference resistance, against the difficulty to get these codes. And within OOC the one coincident with constraints of distance between adjacent symbols (OC1d) [1] are the best example to introduce and test the main idea of frequency synthesizer. Add for this, experimental data is available for the case of OC1d, which could parametrize and normalized the results of simulation. Finally, the chapter concludes with the way for non-coherent detection communications protocols where this type of codes is used.

2.1. One coincidence code with distance constraints

Sequences are widely used in communications, these are founded in applications like corrections errors, cryptography, redundancy introduction, secure hopping systems and channel accessing. The topic in the present research correspond the last applications, frequency hopping (FH) sequences used for FH-CDMA accessing, the set of codes is denoted by $\mathcal{H} = (q, L, \lambda_a, \lambda_b)$, where q is the total symbols (or equivalent available carriers) included in the cyclic additive group of order q: $\mathcal{F} = \{f_0, f_1, \dots f_{q-1}\}$, L is the length of each sequences and λ_a and λ_b corresponds to maximum Hamming auto-correlation sidelobe (with $t \neq 0$) and minimum cross-correlation (1); if $X = (x_0, x_1, \dots x_{L-1}), Y = (y_0, y_1, \dots y_{L-1}) \in \mathcal{F}$ and $H_{X,Y}(t)$ the Hamming classical measure distance is:

$$H_{X,Y}(t) = \sum_{i=0}^{L-1} h[x_i, y_{i+t}], \quad 0 \leq t < L \tag{1}$$

To classify the performance of different families $\mathcal{H}$, considerer $\Lambda(\mathcal{H}) = \max_{X,Y \in \mathcal{H}} (\lambda_a, \lambda_b)$. In the 70's Lempel and Greenberg [28] (2) developed an expression for lower bound and until 2004 Peng and Fang [6] (3) got an expression with more insights in the nature of this type of sequences, respect to length and cardinality. This condition is applicable for set of M sequences, so if $\mathcal{R} \subset \mathcal{H}$ the bounds are expressed by:

$$\max_{1 \leq t < n} \{H_{X,X}(t)\} \geq \left\lceil \frac{(L-\epsilon)(L+\epsilon-q)}{q(L-1)} \right\rceil \tag{2}$$

$$\begin{aligned} \Lambda(\mathcal{R}) &\geq \left\lceil \frac{L(LM-q)}{q(LM-1)} \right\rceil \\ \Lambda(\mathcal{R}) &\geq \left\lceil \frac{2ILM-(I+1)Iq}{M(LM-1)} \right\rceil \end{aligned} \tag{3}$$

Where ϵ is the least nonnegative residue of L module q and $I = \lceil LM/q \rceil$. The set of sequences with these conditions represent *optimal case*, however the construction of the set for any values of L or q could be computationally and mathematically complex to get. Some con-

structions are limited to powers of prime values ($q = p^m$) using algebraic, geometry or synthesis constructions, in some cases and for determined combinations of values the set of elements is very small and only can support a low number of users. The case $\Lambda(\mathcal{H}) = 1$ is the case of outperformance and can be optimized with the additional condition of adjacent symbols with a minimum distance value d.

Bin [1] proposed an algorithm to get families of codes using generators with some properties, with restrictions in the number of symbols q and distance values d. Although this type of codes was designed for RF application case, they received particular attention in the beginnings of optical CDMA, Fathallah [10] developed a hardware implementation for OCDMA using Bragg gratings like encoded elements in the frequency synthesizer and using the codes of proposed by [1].

The Bin's algorithm is based in a continuous (*random*) search of a vector that fulfillment two conditions, although the search of the generator vector F_j is not always successful, the method could find in some cases fast sets of sequences with the Hamming cross correlation value required, restriction of distance between adjacent symbols determines the length of sequence. For example, the family $\mathcal{H} = (29,12,0,1)$ presents 40 different generators, [10] use $g_0 = \{13, 9, 12, 11, 14, 10, 16, 20, 17, 18, 15, 19\}$ like generator and implement the synthesizer with user codes presented below (Figure 1).

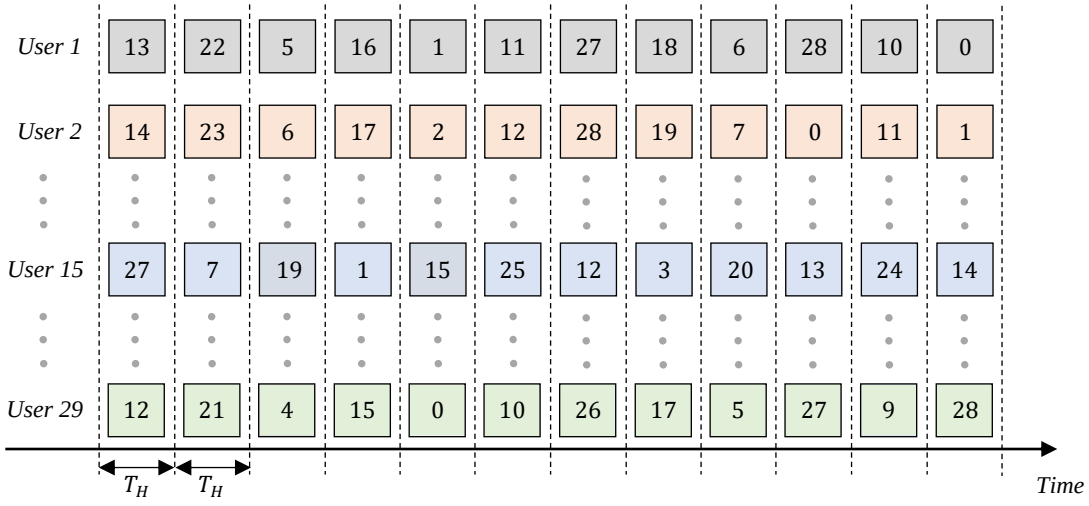

Figure 1 *One coincident code with adjacent distance restriction* The family $\mathcal{H} = (29,12,0,1)$ with distance of 8 between adjacent symbols, the total users could be 29 but the performance for 15 users in OCDMA the

levels of BER are over 10^{-6} . The RF case use each carrier time hopping (T_H) or dwell time. The code family was producing with Bin method and bellows to optimal case.

The use of (OC1d) codes implies the restriction of spectral uses of the frequency and near spectral values, for example the standard IEEE 802.11 (*Bluetooth*®) with $q = 78$ symbols applied the condition for $d > 6$ and use 3 sets of 26 codes for the network, the way to produce this codes is using pseudo random codes. Clearly, with the increase of users the probability of collision between adjacent slot times with the same carrier frequency, increase the false detection probability and finally the MAI of the system.

2.2. Properties and generation

The one coincident (OC1d) sequence set $\mathcal{H}$, with distance restrictions d, has the following properties, with $K = \{f_0, f_1, \cdots, f_{L-2}, f_{L-1}\} \in \mathcal{H}$:

i. All the sequences have the same length L: $card(K) = L, \forall K \in \mathcal{H}$

ii. Each $f_i \in \mathcal{F}$ appear at maximum one time in a code.

iii. The maximum value for H_{XY} is 1 for any value of τ. For $X, Y \in \mathcal{H}$

iv. For all element of the family $K \in \mathcal{H}$, $|k_i - k_{i+1}| > d$

The Bin algorithm [1] is based in a combinatorial search, the hypothetical generator vector $\mathcal{F}_j$ is constructed with cumulative values D_j, the main idea is to find a vector where all the cumulative values are no repetitive. Although for the case of q even is suboptimal, the odd case always produces an optimal family. The $\mathcal{H} = (29,12,0,1)$ family, could be produce an easy way of tens of families using brute force (*randomly*) Figure 2 with a (day of today) commercial PC. The procedure is the following:

For a given q and d, the length of the sequence is $L = q - 2d - 1$, construct a permutation of set $A = \{d + 1, d + 2, \ldots, q - d - 1\} = \{C_1, C_2, \ldots, C_L\}$, in the way that:

a. $C_i + C_{i+L/2} = q$, for $1 \leq i \leq L/2$.

b. $D_1(j) \neq D_1(j) \neq D_2(j) \neq \ldots \neq D_L(j)$, for $2 \leq j \leq L/2$

Where $D_n(j) = C_n + C_{n+1} + \ldots + C_{n+j-1} (\mathrm{mod}\ q)$

The search of the generator $\mathcal{F}_j = (D_1(1) + j,\ D_1(2) + j, D_1(3) + j, \ldots, D_1(L) + j)$, implies a *try-error* method with each possible permutation of set A. With a random approach the algorithm can produce enough list of applicable families codes (Table 1), although it is not the total theorical families, the value converge and the advantage is the possibility to explore the performance of the system respect to the codes family to be used in the final synthesizer. Although the conditions a) and b) do not guarantee equal spectral requirements of the generators $\mathcal{F}_n$, this presents the opportunity to classify the codes in terms of BER and select the best option in terms of synthesizer performance.

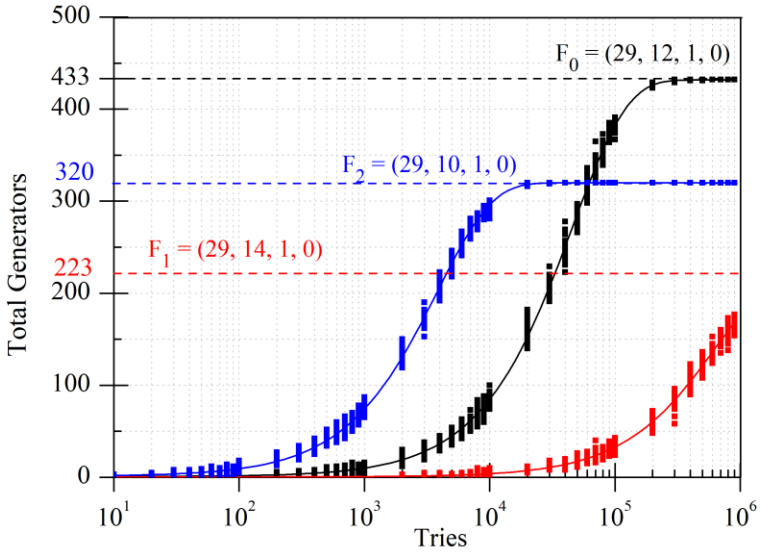

Figure 2 *Try-error method* The System over 100 tries produce certain amount of families, each family has different spectral performances, so the system in general depends over the hardware final construction. The rational fitting produce an asymptotic approach to the maximum family generators, with computing time of less than 1 minute the brute force method can produce all the possible family codes that produce [1]

2D and 3D codes [29] with the requirement to increase of users number require the combination of phase, amplitude or time. Fiber optics implementations increase the attention, but the Bin case represent the top case of 1D codes with best spectral performance for RF CDMA application. To increase the cardinality of codes, Kim proposed an algorithm to insert blank spaces [24], next to generalizing the odd and even values for *L* in Bin algorithm of generators procedure [30], allowing any value for the adjacent distance and extension of codes.

The Kim approach defined the family $K \cup \{\otimes\}$, select a generator similar to the Bin case and select a sequence of time spaces $B_i = \{b_0, b_1, \dots, b_i, \dots, b_k\}$ where b_i represents the number of spaces to insert between D_i and D_{i+1}, the new $C^{D,B} = \{s^{(0)}, s^{(1)}, \dots, s^{(q-1)}\}$. The new cardinality is $2q$ against the q initial value. However, the time in encoding or decoding system decrease the transmission rate.

q	d	L	Time (s)	Total $\mathcal{F}_j$	Generator Bin [1]
7	0	6	10	7	1 3 2 6 4 5
7	1	4	10	4	2 3 5 4
9	0	8	10	~	non-existence
9	1	6	10	~	non-existence
9	2	4	10	4	3 7 4 0
11	0	10	30	17	1 2 4 8 5 10 9 7 3 6
11	1	8	30	~	non-existence
11	2	6	60	9	3 4 6 8 7 5
13	0	12	60	22	1 2 4 8 3 6 12 11 9 5 10 7
13	1	10	60	~	non-existence
13	2	8	60	14	3 5 6 4 10 8 7 9
13	3	6	20	9	4 5 7 9 8 6
15	1	12	60	~	non-existence
15	2	10			3 9 7 4 5 12 6 8 11 10
15	3	8			4 6 7 5 11 9 8 10

Table 1 *Comparison random search algorithm using Bin approach.* The computer power has had a real advance in the last years, so the comparison on time is no proportional to Bin table several families of codes implied different performance (Tries for this case is NT = 1000000).

Although the OC1d were initially designed for RF-CDMA case, the first attractive applications occurred by Fiber Optic CDMA or OCDMA, in fact, Fathallah developed a hardware implementation using Bragg gratings like encoded elements in the frequency synthesizer, additionally conclude about of time insertions: "*physical spacing between gratings reduces the probability of coincidences between users*" [10].

The arbitrary time delay introduced by Kim exploits this idea, however the case supported mathematically by Kim required spaces of constant time (constant length of fiber optics for

OCDMA). From the point of fabrication, the separation between symbols is easily changed and could be adjusted both in fiber optic and RF microwave transmission lines, which is the case presented here.

Before to include the insertion of time, it is necessary to include the parameters to compare the different families or generators, the description of the synthesizer and measure methods are presented based on previous literature results.

2.3. Synthesizer in OCDMA

The correlation detector hardware proposal by Fathallah [10] correspond to an array of Bragg gratings, spectral distance and spatial positions are provided by OC1d (Figure 3). optical pulse is inserted in port A and sequence of frequency reflecting carriers are produced in port B, hopping velocity is limited by distance between adjacent FBG; the encoding is based in FBG with uniform apodised and coupling coefficient $\kappa_0 = 220, \mathcal{H} = \{29,12,0,1\}$ with generator $G_0 = (13,9,12,11,14,10,16,20,17,18,15,19)$.

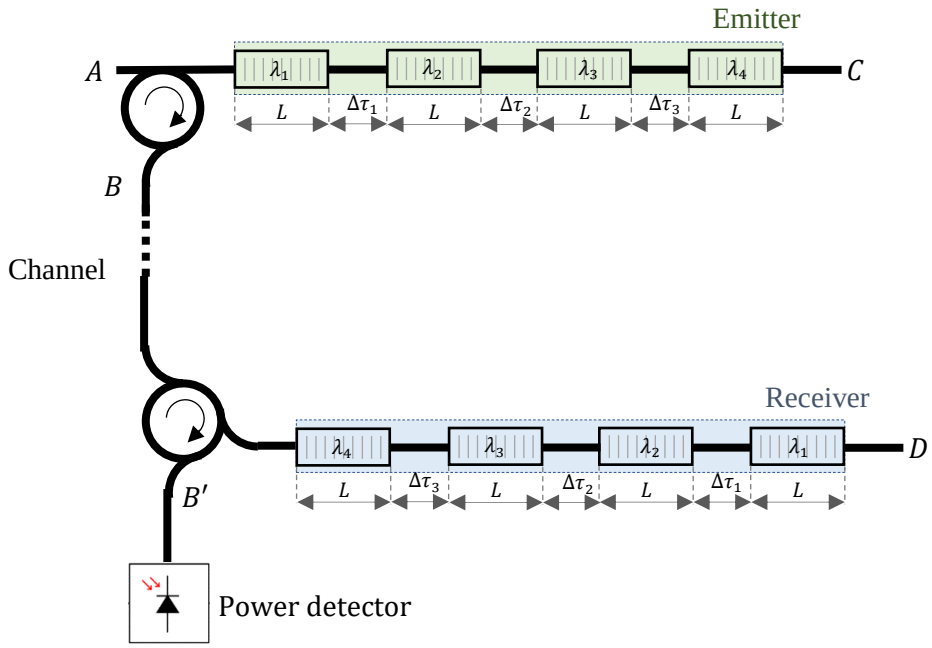

Figure 3 *Optical Frequency synthesizer* Port A is the input signal, C and D is an absorbing mechanism due to reflecting nature of FBG, B is the output or connection to communication channel and finally the correlational detector is provided by a power detector. The figure shows a code with fourth symbols and time delays between adjacent resonators. The order on the receiver is just reverse in the emitter order

The reflectivity profile for Bragg grating case is given by the expression (4), where κ_{ac} is the ac coupling coefficient, L is the length of FBG, δ and α are variables related with the apodization function [31]. The apodization profile presented by Fathallah in [10] contain the sinc case and parameters of synthesizer are specified.

$$\rho(\lambda, \mathrm{L}) = \frac{-\kappa_{ac}\, sinh(\alpha L)}{\delta\, sinh(\alpha L) - i\, \alpha\, cosh(\alpha L)} \tag{4}$$

Optical pulses enter in A, travels between each Bragg grating with a defined $\rho(\lambda, \mathrm{L})$ profile (Figure 4) and the sequence is transmitted by port B over the optical circulator (C correspond to absorber element). To decode, the sequence order is inverted, and the output final signal is compared by a threshold in port B' using the power detector. The detection is completely asynchronous, and the interference arrived of another encoder users increase noise floor and in consequence false alarm for the communications process.

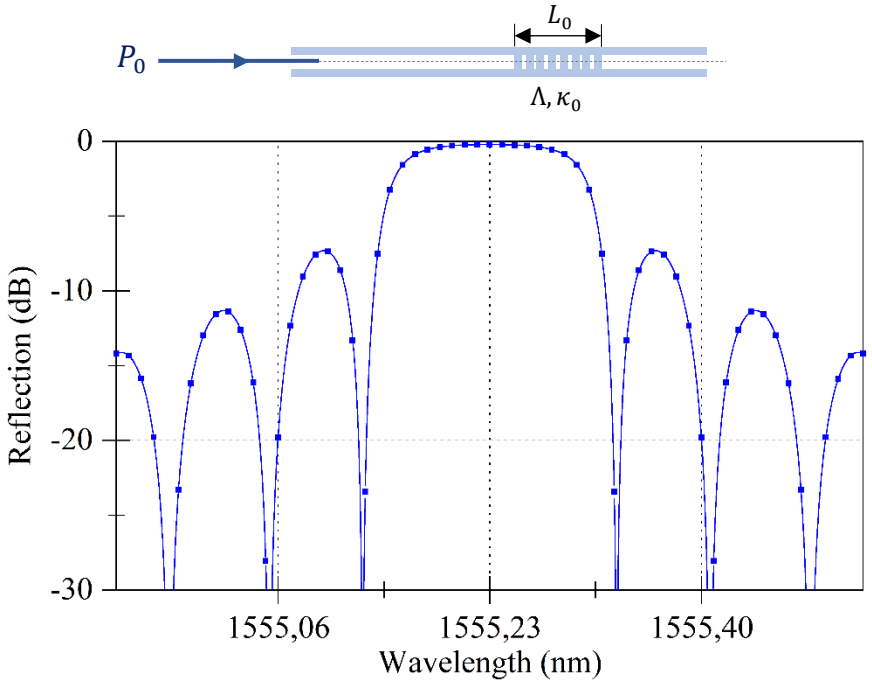

Figure 4 *Uniform apodized FBG* The adjacent symbols are vertical gridlines, for the uniform case this is the final second lateral lobule, the adjacent interference is causing interfering power for total MAI, in fact the Bin algorithm required minimum distance between adjacent symbols, the analyzed case by Fathallah [10] select 8 like spectral distance between consecutive symbols

To calibrate the simulation performance of the codes the data provided by Fathallah allows to normalize the data. So, it is necessary to include the main parameters based fundamentally in BER and cross correlation values. The worst case considered is based on all the signals arrived at same phase, this case has low probability and in some researches the value of BER is less, however, this represent the worst scenario to work.

2.4. Quality Measure

The energy on the power detector (Figure 3) could be expressed like superposition of the all the income signals, for the case of CDMA the user x send the information encoding with the respective orthogonal code, the signal over the channel could be expressed by (5), $d_{k,j}$ represent the binary value encoding in the user sequence of code, L is the length of the code and $p_j(t)$ is the impulse response to the Bragg grating which in frequency domain is presented in Figure 4.

$$x_k(t) = \sum_{j=1}^{L} d_{k,j} p_j(t - jT_c) \tag{5}$$

If the channel there are K active users, the superposition of signal on the receiver $r(t)$ (6), with τ_k the phase difference between each signal, in this case the worst scenario is $\tau_k = 0$ for all the users signal and b_k represent the binary value.

$$r(t) = \sum_{k=1}^{K} b_k x_k(t - \tau_k) \tag{6}$$

The power input on the receiver $P(t)$ (7) generally is due to power detector with integral energy over the total time symbol, if the user 1 has the code $c_1(t)$ the input can be expressed like the following expression:

$$P(t) = \int_0^T c_1(t) r(t) dt = b_1 \int_0^T \big(c_1(t)\big)^2 dt + \sum_{k=1}^{K} b_k \int_0^T c_1(t) c_k(t - \tau_k) dt \tag{7}$$

The first term on the right side correspond to energy of the effective information and the second term is the energy of the interference between users respectively (MAI), the key of the orthogonal codes is to decrease the energy coming from the cross-correlation function,

another parameter to considerer is the delay element between adjacent symbols τ_k which introduce asynchronous from another signals. The element to minimize is the interference part, i.e. the cross-correlation function between each user code (8), for now we are going to considerer elements in a more general sense.

$$\langle c_i, c_k \rangle = \int_0^{T_{max}} c_1(t) c_k(t - \tau_k) dt \tag{8}$$

Where T_{max} corresponds to the maximum duration of the pair of symbols T_c, equivalently chip time for analogous CDMA case, plus the time physical separation $\Delta\tau_i$. taken each pair of codes to get the variance (9), where the x value corresponds to energy in a defined time and $f_X(t)$ is the cross-correlation power signal.

$$\sigma_x^2 = E(X - \mu_x)^2 = \int_{-\infty}^{+\infty} (x(t) - \mu_x)^2 f_X(t) dt \tag{9}$$

The cross-correlation functions for power signals for discrete case have described by the expression (10), the evaluation to include the spaces between adjacent symbols require time dependence or semi-continuous, so the value M in (10) represent the number of points to considerer and not the length of the user code.

$$\rho_{XY}(l) = \lim_{M \to \infty} \frac{1}{2M + 1} \sum_{n=-M}^{M} X[n] Y[n - l] \tag{10}$$

To normalize the cross correlation is using the two following expressions:

$$\begin{aligned} \rho_{XX}(l) &= \frac{r_{XX}(l)}{r_{XX}(0)} \\ \rho_{XY}(l) &= \frac{r_{XY}(l)}{\sqrt{r_{XX}(0) r_{YY}(0)}} \end{aligned} \tag{11}$$

The average power of each user can be expressed by the following expression (12), where $\mathcal{E}(\cdot)$ is the mathematical expectation. The detector is directly the cross-correlation function, so the mean power received is under the correlation function. For example, the family $\mathcal{H} = (29,12,0,1)$ using the parameters in [10] produce the power interference profile presented in

Figure 5, the central peak is the value to optimize against the adjacent peaks which are provided by the power of another encoders users, finally although the codes are one coincident, increasing the number of user produce superposition of adjacent peaks of another codes.

$$\mathcal{E}(|\rho_{XX}(t)|^2) = \sigma^2_{\rho_{XX}} + \left|m_{\rho_{XX}}\right|^2 \tag{12}$$

The main hypothesis of this research is to find a way to decrease the MAI interference including random spaces between adjacent symbols, this method spread the noise of lateral cross correlation power values, the case presented in Figure 5 do not use adjacent spatial values.

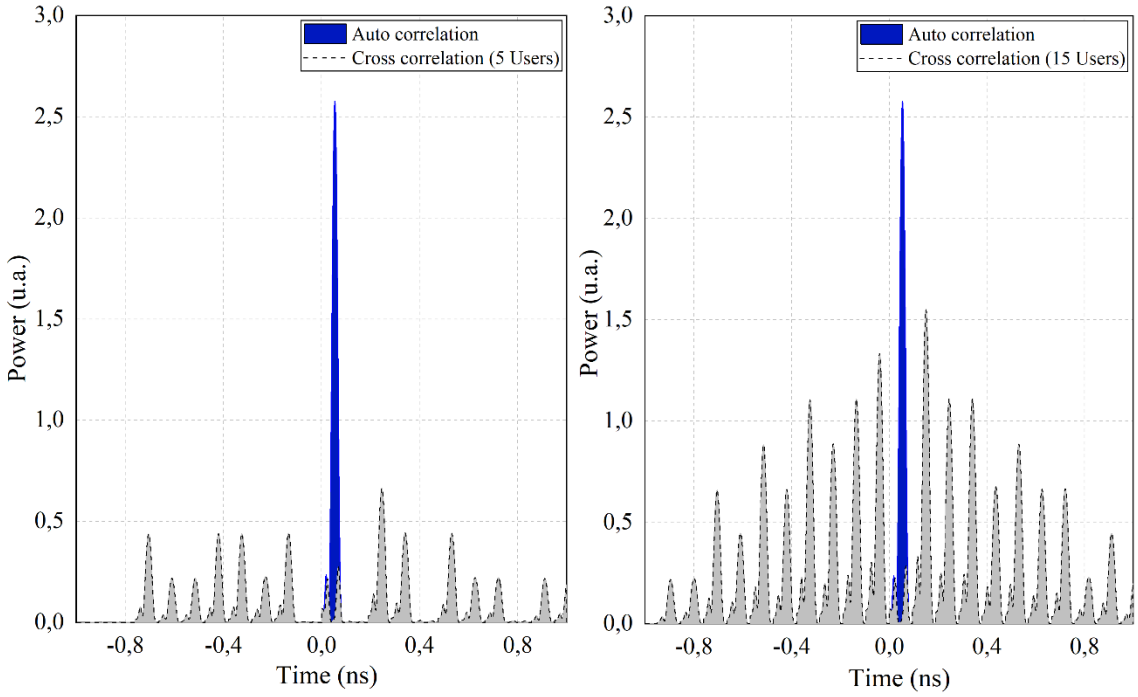

Figure 5 *Performance for family* $H = (29,12,0,1)$ *in OCDMA* Clearly with 15 interferers the cross-correlation lobules generating false errors of detection, this adjacent lobule is almost the half of power of main line. This result is was calibrated using data by Fathallah [2]

The SIR (13) is an important entity in communications to indicate the quality of link between a transmitter and receiver in a multi transmitter-receiver environment. If the system has N nodes inside the network which simultaneously can transmit and receive at the same time using the same channel, the received SIR could estimate with the following expression at receiver i with N active elements:

$$SIR_i(k) = \gamma_i(k) = \frac{g_{ii}p_i(k)}{v_i + \sum_{j=1,j\neq i}^{N} g_{ij}p_j(k)} \tag{13}$$

Where $p_i(k)$ is the transmission power of transmitter i at time step k, g_{ij} is the link gain from transmitter j to receiver i and v_i represents the receiver noise at receiver i There some techniques to estimate the SIR value, gaussian approach overestimate the BER values, in this case, it will assume the probability of access to channel using the normal approach, so the SIR could be written by the expression (14), where $\bar{\sigma}^2$ is the main value of (9), taken of each pair of codes of all possible combinations.

$$SIR = \frac{N^2}{I_T^2} = \frac{N^2}{(K-1)\bar{\sigma}^2} \tag{14}$$

Assuming normal accessing to the channel and independent users, the probability of error is represented by the expression (15), the final performance of the channel is presented in Figure 6, the case of no spatial insertion generate a value of error superior to the case of introducing constant values between adjacent symbols, however the family of codes presented by [10] it is not the only one and with the metrics presented by the (9) (10) and (15), we can

$$BER = P_e = Q\sqrt{SIR} = \frac{1}{2}\text{erfc}\left(\sqrt{\frac{SIR}{2}}\right) \tag{15}$$

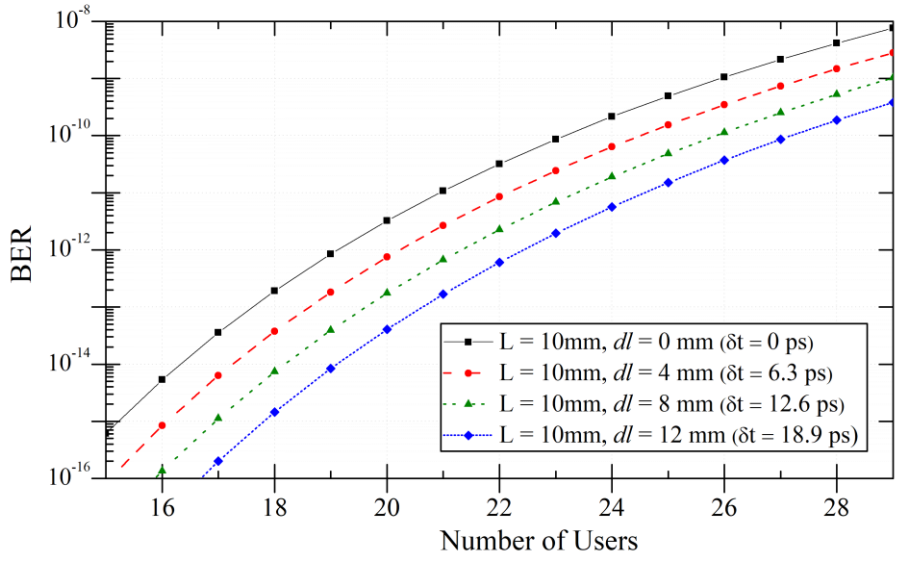

Figure 6 *Insertion of spaces between adjacent symbols.* The insertion of spatial separation $\Delta\tau_i$ in synthesizer (Figure 3) improve the response over the final BER in the communication system. However, increase the separation implies a chip time (T_c) longer. The initial proposed separation in [10] is 8 mm, with a length in the Bragg grating of 10mm.

proceed to check the complete family generator $\mathcal{H} = \{29,12,0,1\}$. Previously to this, we need another notation $\mathcal{H} = (q_0, L, k, \tau, \max(H_{XY}), \max(H_{XX}))$, where k is the number of blank spaces and τ is the spatial distance between adjacent encoding Bragg gratings. For $k = 0$, the family is reduced to Bin approach, but for simplicity using $\mathcal{H} = \{\mathrm{q}, \mathrm{d}, 0,1\}$ for OC1d case, in real implementation $\tau \neq 0$ and generated a little improvement over the synthesizer response.

Performance of introducing white spaces using [30] is shown in Figure 7 and Figure 8, Bin approach comparison clearly exhibit a distinction between spectral response and increase time delays behaviors, both elements allow to control the final BER on the synthesizer detection, but the delays introduced by the white spaces it is not enough to control the rise of sidelobes in cross correlation function, in fact, the family *B* (Figure 7) which use insertion of blank spaces, increasing the user number but cross correlation behavior (Figure 8) with 25 users produce equal proportion of valid and incorrect data. On the other hand, family *D* requires double carriers, but in terms of spectral conditions over performance the behavior of D, even with minimum physical separation between each encoder resonator.

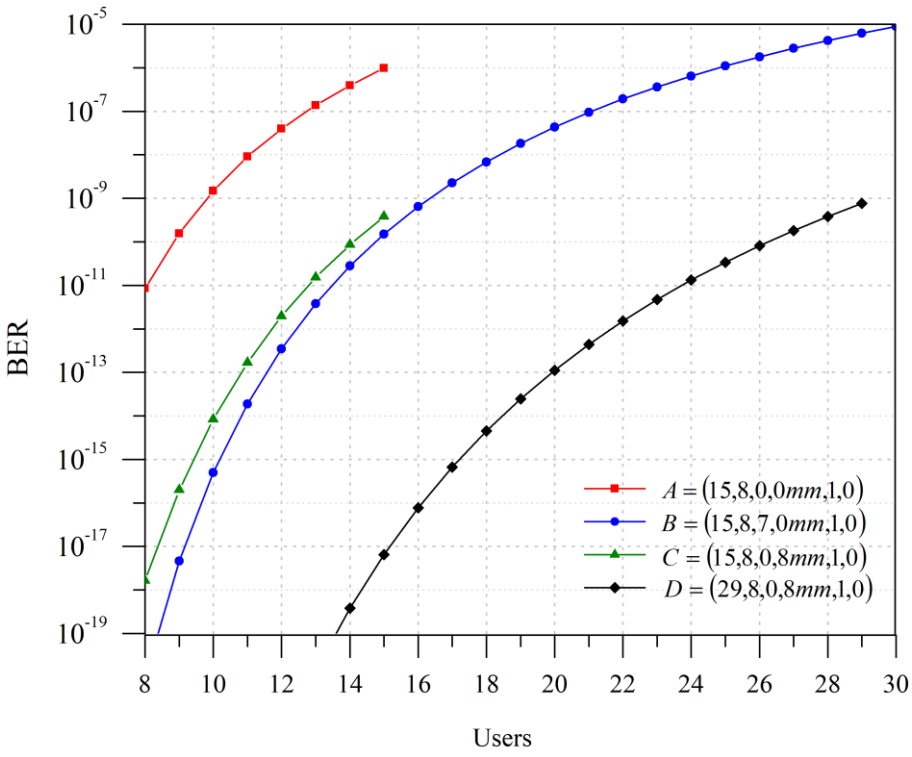

Figure 7 *Blank insertion against spectral numbers* Insert blank spaces, although increase the number of user, the performance in terms of BER is at least the same that include only spatial separation, like C and D families, however the increase of user numbers is another topic to improve.

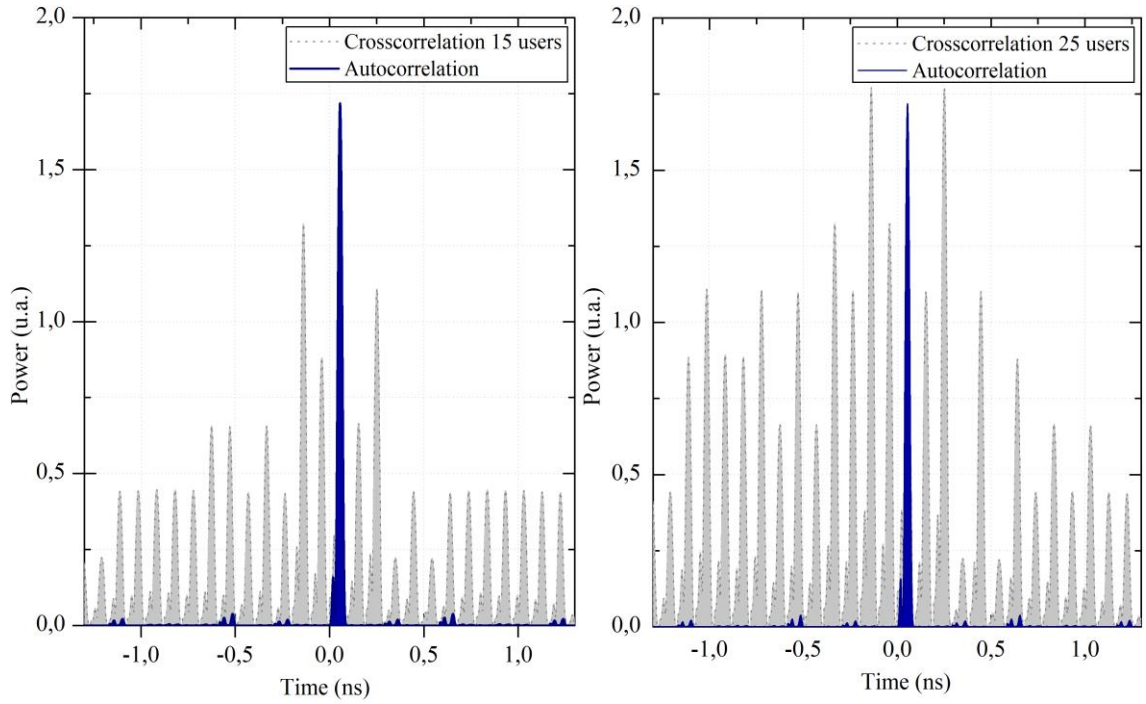

Figure 8 *Kim Codes performance on time domain.* On the left, the cross correlation using the code belong to the family $\mathcal{H} = (15, 8, 7, 0.0\ mm, 1, 0)$ with 15 interferers and on the right corresponds to 25 interferers for asynchronous case. The predictions over Figure 7 show a bad performance, with near of 15 users the BER is below to 10^{-7} inferior to limit of multimedia requirements in OC3 standard.

Another way to inspect the impact the sharing channels, due to increase user number, is the rise in the level of noise floor tending to reducing the dynamic range in channel communication (Figure 8). Clearly, to decrease $\bar{\sigma}^2$ one way is using more time in the total length of the chip time or improve the spectral values, i.e. equivalent to increase the number of frequency symbols.

The Hamming cross correlation function is a discrete measure of coincident slot frequencies, but in continuous time domain, dynamic range is a direct parameter over detector to include in BER calculations, so some parameters of the resonators are required to be included, specifically the spectral response, time physical delays and the power detection profile, for the present study the distribution of spaces is the main objective. The limitation for the FFH OCDMA, showed with family B in Figure 7, is the delay time between FBG, introduction blank spaces decrease the bit rate, increase the user number but even that, adjacent cross correlation peaks increase proportional with the user number (Figure 8).

Before to introduce the random distribution of distances between adjacent symbols, the response of each family's element $\mathcal{H} = \{15, 8, 0, 0.0\ mm, 1, 0\}$ is generally a little bit different, so the comparison introducing the random spaces will be use the best generator belongs to family, in fact Figure 9, generators belongs to $\mathcal{H} = \{29, 8, 1, 0\}$ contains small range of changes close to fractions of an order of magnitude.

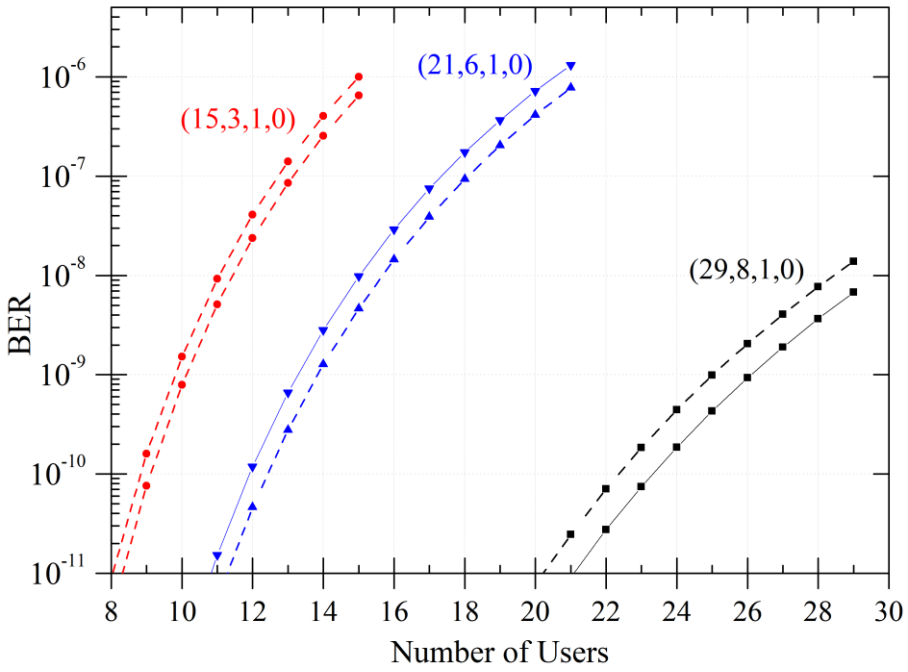

Figure 9 *Generators performance comparative* The generators applied over the OCDMA case performs a little bit different over the system, so there are optimal generators inside the optimal OC1d cases, the main suspect is around the final spectral response.

2.5. Random delay insertion

The main hypothesis of this research is that inclusion of delay time like [24] but only the equivalent physical spaces, not using the equivalent space of the Bragg grating length, reduce the conflictive peaks over cross correlation detector, but distributed randomly, this spread the sidelobes peaks over the cross correlation, increasing the dynamic range and thence increase the BER in communication protocol.

Clearly, the extension of delays between adjacent symbols reduce the data rate transmission, but physically, this spaces are required for the construction of FBG process [13], initially the insertion times are equals spaced, in the structure on Figure 3, the length spaces present

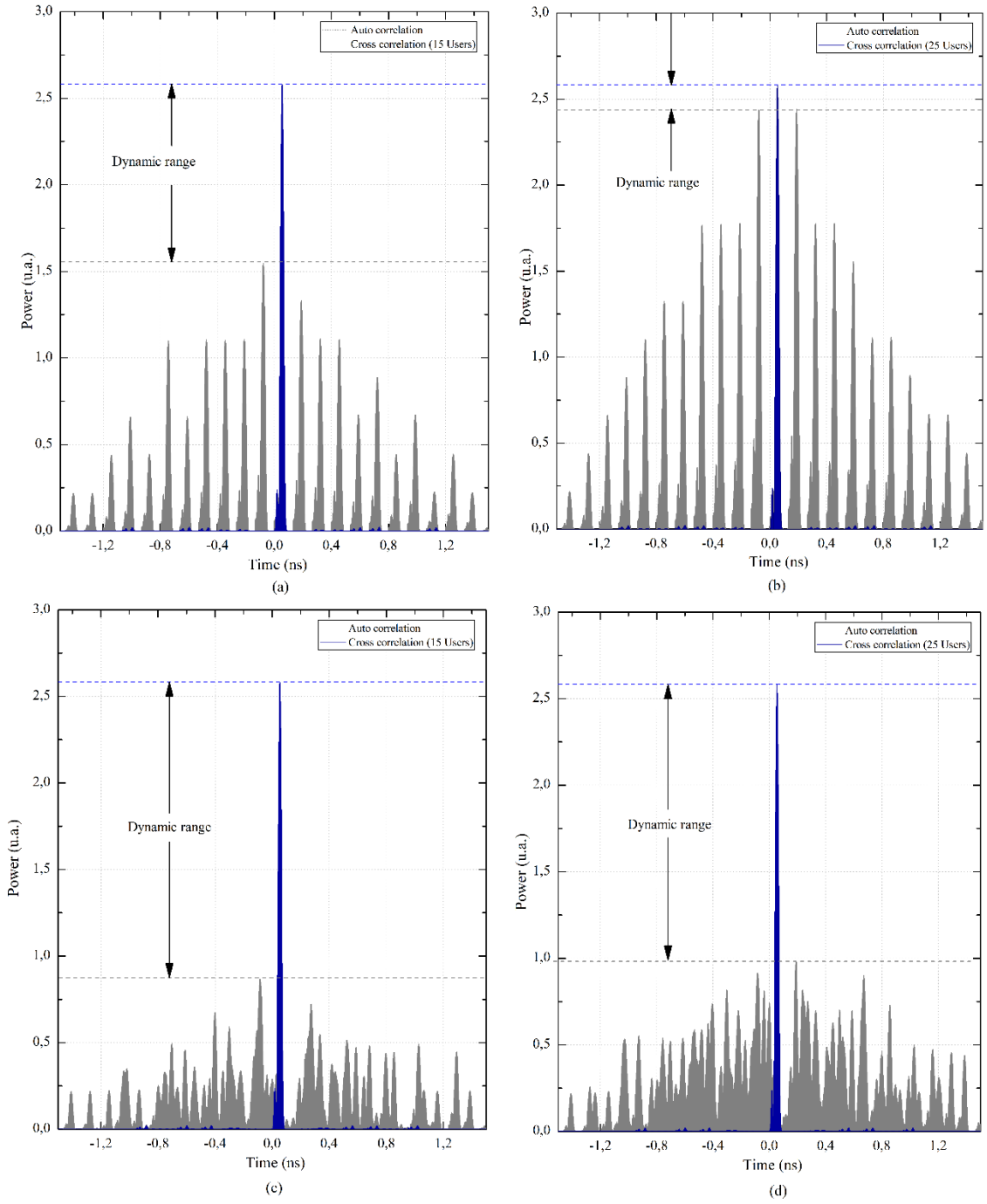

Figure 10 *Random spaces cross correlation.* In time domain, using the family $\mathcal{H} = \{29, 8, 0, 4\ mm, 1, 0\}$ the performance is evaluated, the insertion of random times distribution between symbols allow to reduces the lateral lobules in cross correlation (a) and (c) compare the case of uniform vs random distribution of spaces, the sparse of power using 25 users in (b) and (d) produce an clear example where the some adjacent peaks could produce false detection bits, in (d) the blank spaces of (b) are spread with power, this is equivalent to reduce the maximum power in one coincident cases, which represent the insertion of noise.

uniform distribution for $\Delta\tau_i$, so for each user we need to define the user code like a composition of spectral sequences plus the distribution of spaces between adjacent symbols (16).

$$\tilde{C}_i = \left\{ \begin{matrix} (f_0, f_1, f_2, \dots, f_{L-1}) \\ (\Delta\tau_{i0}, \Delta\tau_{i1}, \Delta\tau_{i3}, \dots, \Delta\tau_{iL-2}) \end{matrix} \right\} = \left\{ \begin{matrix} C_i \\ \tau_{i(L-1)} \end{matrix} \right\} \tag{16}$$

The requirements of random time distribution is to generate values in such a way that side lobes of cross correlation decrease the energy value and spreading over the delay empty spectral cases, this problem has several similarities with Golomb ruler problem [32] and partitions generation [33], practical use is for channel allocation frequency to reduce intermodulation interference [34], radio antenna placement [35], cryptography [36] and four wave mixing crosstalk in DWDM [10]. The generation of this spaces reduces the probability of matching the only one coincident case between two sequences, that corresponds to maximum condition that contain cross correlation C_i and the main cause of rise some lateral peaks (Figure 11).

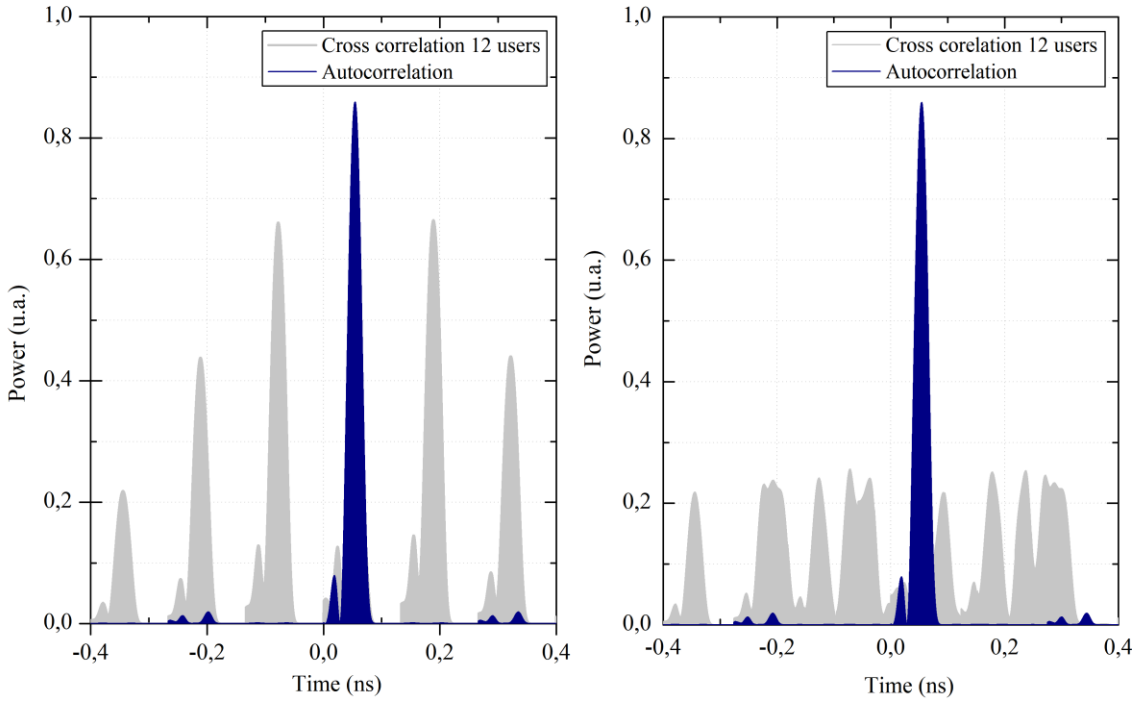

(a) (b)

Figure 11 *Random spacing*. With 4 spectral components the reduction of sidelobes is presented and dynamic range increase. The spreading phenomena clearly reduces the (a) high peaks in uniform time distributions and with (b) random time distribution avoid the superposition between one coincident case in the cross-correlation function.

The family considered here $\mathcal{H} = \{13, 4, 0, 4\ \text{mm}, 1, 0\}$, clearly with shortest length of code, decrease the probability of find a high lateral lobule in cross correlation function, but one coincident case implies that main lobule is at least fourth times the power of one coincident case, which ostensibly reduce dynamic range. The optimal generator found it for this case is $\mathrm{G}_0 = (5, 6, 8, 7)$, with all the users sharing the channel (Figure 11a) and with uniform separation between symbols, increase probability of false alarms, but again introduce randomly length separations, reduce at maximum one coincident case for the superposition of all users (Figure 11b).

For now, it was used methods used in OCDMA, the response for RF is not equal in the sense of using different RF resonator and material characteristics, however, even considering propagation on conductive transmission lines, combination of random delays using cross correlation encoders improve the detection method, allowing to share the channel without decrease the QoS against increasing the user number.

2.6. Summary

The OC1d were introduced within their mathematical properties and algorithm generation. Main results arose from OCDMA and with the synthesizer of Figure 3 some families of sequences had been detected to produce better performance. Exploring the insertion of time, delay spaces produce an even known result of increase the number of users [24] but the sidelobes of cross correlation is still increasing, so the dynamic range is strongly affected, one way to reduce this peaks could be done spreading this energy in not concurrent spaces, affecting the one coincident conditions but in time domain.

Chapter III

Planar Resonators in Microwave Technology

The implementation and testing of orthogonal codes using Microwave technology allows to differentiate each user in time and frequency domain analog to fiber optic case with similar spectral and time scaled characteristics. The main limitation of using passive elements is the requirements of high-quality values (Q), or equivalently to high selectivity spectral elements. Conversely, the high integration of passive elements, compatibility with RF industry techniques of fabrication, reproducibility, standard methods of calibrations and measurement, makes the planar transmission lines (PTL) a choice to check rapidly structures like the synthesizer proposed.

Although, there are a lot of structures, geometries and studies about resonators on microwave substrate, recently it appeared new models and studies supported at present by a lot of applications; design of filters, antennas for 5G applications, superconductor resonators for quantum computations, microwave kinetic inductance detectors, sensing abilities among others. The technology selected in this research was Microstrip. However, the control of impedance is a little tricky against Coplanar Waveguide (CPW). the technology allows a high range of parameters like impedance and has a high compatibility with PCB fabrication in the electronic industry.

This chapter contains the basis of Microstrip technology applied for fabrication, characterization and testing of the resonators. The first two sections explore the basis of propagation in this technology within the dependences of geometry and materials properties. The circuit analysis allows to interpret the coupling factor and the limitation of the capacitance and its delicate design to improve the Q final value.

3.1. Planar Transmission Line Resonators

In relation to another type of technologies for fabrication of resonators, the final Q factor is very limited using only transmission lines (Figure 12a). Two of the major limiting factors are: the losses due to substrate and conductor materials and the mode of propagation in this technology, where the quasi-TEM mode finally is concentrated in a finite section of a material (Figure 12b), resulting in a limit frequency for propagation. On the other hand, the process of fabrication in thick films is standard and well characterized with conventional techniques like lithography, laser ablation or mechanical machining.

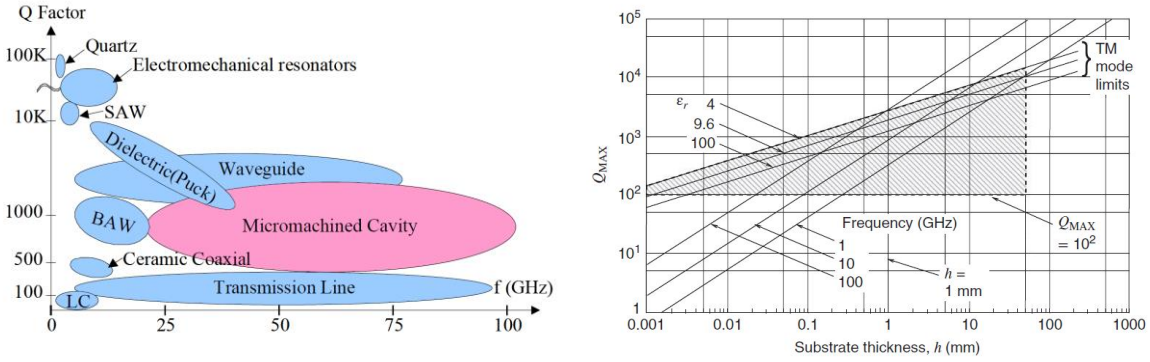

(a) (b)

Figure 12 *Performance of resonator techniques classified by* (a) technology of fabrication [37] and particularly the case of Microstrip (b) [38], where the limit is based on the mode of propagation and losses on commercial substrates and standard temperatures of conduction.

The two situations mentioned above limit the performance of the final symbol (resonator) in consequence, the synthesizer function, and the hardware requirements to test. The Q factor is deduced directly from the bandwidth (δf) (17) and the separation between adjacent symbols, so the model of the resonator is essential for the final design. The Q factor is defined by expression (17), which express in general the quality factor for the system. In planar circuits, β corresponds to propagation constant, f_0 is the resonant frequency, δf is the bandwidth and α is the attenuation constant, which include radiation losses (α_r), dielectric losses (α_d) and conducting losses (α_c).

$$Q = \frac{f_0}{\delta f} = \frac{\beta}{2\alpha} \tag{17}$$

For the frequencies of interest, the radiation losses can be neglected, only the conduction and substrate part are determinant for final value of Q. The commercial substrates for RF industry have metallization of Copper and values of $\tan\delta \sim 10^{-3}$, so the limits for quality are nearly hundreds for planar circuits, i.e. Rogers® materials like RO4350B (Figure 13) and RO3010 using microstrip technology allow high ranges of impedance with cutoff frequencies of 50 GHz, increasing the frequency increase the losses mainly in the conductor part, but decrease the dimensions of the system. For the frequencies and materials used, the primary source of losses is the conducting part, finite conductive copper limits this value.

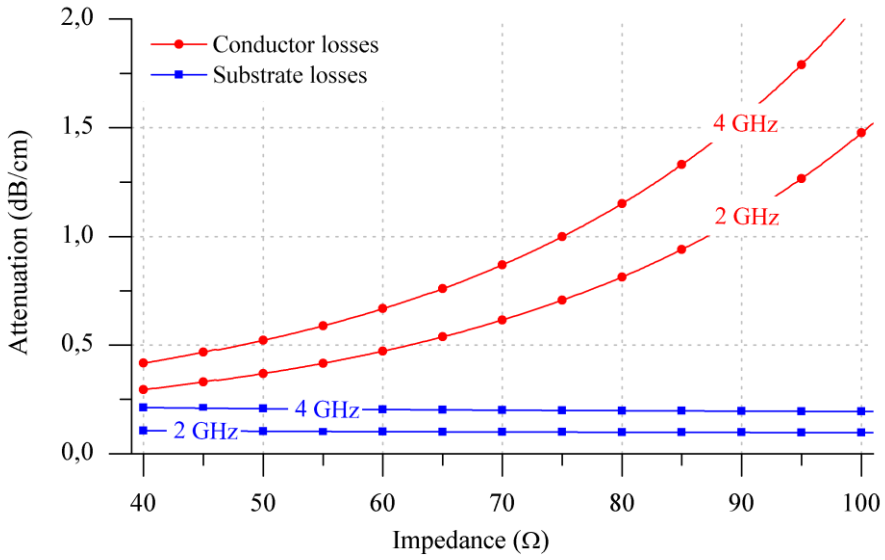

Figure 13 *Losses for different frequencies* using like example RO4350B substrates (Copper of 17.5 μm and substrate profile of 0.51 mm), the characteristic impedance in microstrip technology is mainly a function of geometrical and material parameters

From the point of view of microwave technology, the resonator can be analyzed using three ways: distributed elements, lumped elements, and physical model. Approximately near to the resonance, the resonator is equivalent a LCR circuit, so all the energy loaded in the capacitor part is passed directly to inductor part, if the system does not have resistance or impedance associate a medium, the interchange of energy could be stablishing like an ideal oscillator.

Clearly, the energy of electric field and magnetic field are the same and the total energy saved in the circuit is given by the expression (18).

$$U(t) = U_E + U_H = \frac{1}{2}LI^2 + \frac{1}{2}CV^2 \tag{18}$$

Where the first term refers to magnetic energy and the second one electric. The quality factor physically represents the capacity of the system to transmit/receive energy in a frequency ω (1), where $\overline{U}$ is the average energy stored and U_{Loss} is the rate of loss energy for the system. So, in a perfect system without losses the quality factor tends to high values. For optical resonators, the quality factor is in order of 10^7 and for superconducting planar resonators in microwave frequencies tends to the same order.

$$Q_0 = \omega \frac{\overline{U}}{U_{Loss}} \tag{19}$$

For the planar resonator, the ways to dissipate the total energy $U(t)$ is by using two factors: pure resistive part α_c and the dielectric losses α_d. Using the equivalent lumped elements and the relation (18), the internal quality factor and resonance frequency of the resonator could be expressed respectively by:

$$Q_0 = \frac{1}{R}\sqrt{\frac{L}{C}} \quad \text{and} \quad \omega = \frac{1}{\sqrt{LC}} \tag{20}$$

Another way to express it is by using a relation between the two independent losses (21). Figure 13 indicates for small conductor widths, the conductor quality factor limited the final performance of the resonator and for microstrip conductors widen the substrate is the limiting part. The internal quality factor could be expressed by the parallel combination (21) of the two quality factors, conducting and substrate.

$$\frac{1}{Q_0} = \frac{1}{Q_c} + \frac{1}{Q_d} \tag{21}$$

This relation of quality values is valid for the case of resonator isolated from the physical world, Q_0. For planar circuits, the coupling is capacitive through feedlines or waveguide

coupling. So, the final value of Q, denoted by Q_L must include the internal physics of LCR system, Q_0 and the coupling external effects Q_e. Or a parallel combination of both systems (22). This dependence with the external part will be explored in the next section.

$$\frac{1}{Q_L} = \frac{1}{Q_0} + \frac{1}{Q_e} \tag{22}$$

Referring to the planar structures, a few advantages of using these technologies are the possibility to integrate the synthesizer with another systems, use standard methods of characterization of Microwave Technology industry and using techniques of fabrication for electronic industry.

The resonance in this type of structures exploits geometrical interference in $\lambda/2$ or multiples of this one. There are a lot of geometrical structures to produce resonance, from fractals to standard linear in transmission or reflection case depending on coupling method, Figure 14 shows the response of a linear resonator with capacitive coupling.

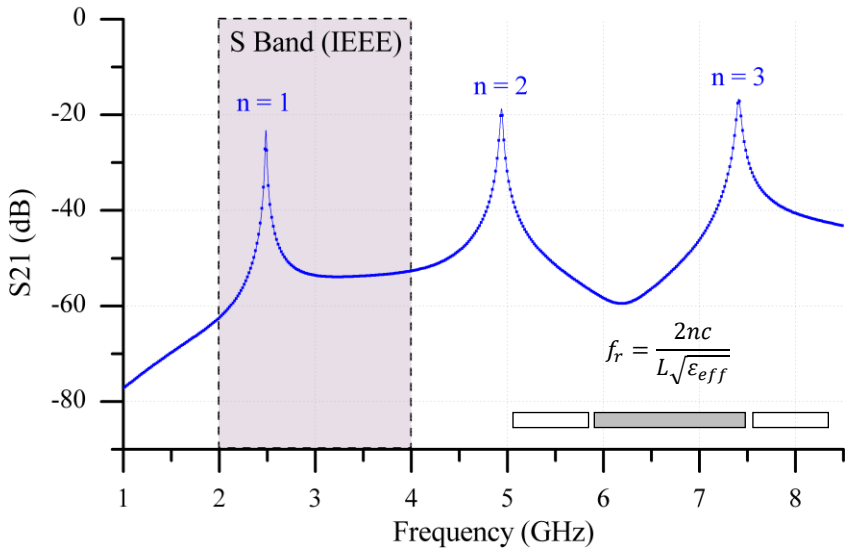

Figure 14 *Linear resonator* The frequency response is multiple of main mode ($n = 1$), this was simulated in CST Microwave Studio using RO4350B like substrate and length dimension of 36.5 mm and gap of 0.25mm. The loaded quality factor is higher for the first modes of resonance in part by the losses increase, reducing of 180 to 160. The S band sector contain a free part correspond to ISM ($2400 - 2483.5\ MHz$).

This type of structure has been extensively researched for posterior implementation of classical design of filters, resonance is presented in multiples of half wavelength, however the

present research is focused on S band, mainly the free bands inside of this last band. Construction of high selective resonators is a hot topic recently due to different interest where is required high sensibility exploiting changes in resonant frequencies, that is in areas like quantum superconducting for qubit detection, electron spin resonance, electro optics conversion and exploiting high sensitive sensing techniques.

3.2. Microstrip Transmission Line

A transmission line is any structure that allows transfer electromagnetic energy of a point to another one [39], this structure could be from an empty space until geometrical arrays of dielectric and metal. There are a huge variety of structures (Table 2) and depending on frequency or applicability, some structures are better ones than others. Among the planar structures used in MIC, Microstrip technology has several advantages to implement Microwave structures, within them the easy way to test and implement systems.

One of the biggest challenges to research in resonator technology is its selectivity or Q_L factor. To understand the quality factor, the main characteristics of microstrip technology will be analyzed, their main constitutive parameters and tradeoffs to finally design the synthesizer.

Transmission Line	**Frequency range (GHz)**	**Impedance Level (Ω)**	**Q factor**	**Potential for low-cost production**
Rectangular waveguide	< 300	$100 - 500$	High	Poor
Strip-Line	< 10	$10 - 100$	Low	Good
Microstrip	< 100	$10 - 100$	Low	Good
CPW	< 60	$40 - 150$	Low	Good

Table 2 *Waveguide transmission lines*. Within the structures with high Q values, the rectangular waveguides and dielectric structures has the better option to selectivity, add to that the modes of propagation allow the system to have less losses than planar cases. Data taken from [40]

Microstrip structure is a substrate with ground plane in one side (Figure 15), the conducting part is above of the ground. The main limitation of this structure is the requirement of a through hole of the substrate to connect ground inside a circuit. Losses in this structure are related to conductor (α_c), dielectric (α_d) and radiative (α_r) parts, for the S-band and materials used the Q factor depends on α_c (Figure 13).

The second limitation of microstrip technology refers to quasi-TEM mode and lowest order surface wave, so the frequency and bandwidth is a limitation for the circuit. However, one of the most attractive advantages is the high library disposal for the construction of elements like power dividers, combiner, lumped elements and so on. Analog to this, the disposal of electromagnetic models for computer simulations, the variety of Electromagnetic CADs using Microstrip models, like Keysight ADS®, Microwave Office (AWS), XFdtd®, Ansoft HFSS® and CST Studio®.

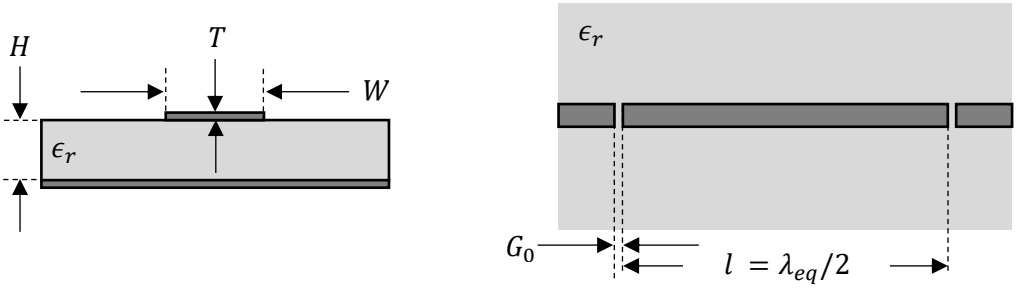

Figure 15 *Microstrip linear resonator* The structure is designed to half wavelength (λ_{eq}), this value depends on geometrical parameters explored in another sections of this chapter and material dependence.

The classical model to characterize the Microstrip technology is given by the expressions (23)-(25). Although these relations are a static approximation (within 0.6% [41] of error, analytical solutions in Electromagnetism are a little bit canonical cases), there are factors not included; enclosure disposal, dispersion on substrate and nonlinear behavior of materials.

$$\varepsilon_{eff} = \epsilon_r - \frac{\epsilon_r - \epsilon_e}{1 + P(f)} \tag{23}$$

$$\epsilon_e = 1 + \frac{\epsilon_r + 1}{2} + \frac{\epsilon_r - 1}{2} F\left(\frac{W}{H}\right) - \frac{\epsilon_r - 1}{2} \frac{T/H}{\sqrt{W/H}} \tag{24}$$

$$Z_0 = \begin{cases} \dfrac{60}{\sqrt{\varepsilon_{eff}}} \ln\left(\dfrac{8H}{W} + \dfrac{W}{4H}\right) \\ \dfrac{120\pi}{\sqrt{\varepsilon_{eff}}[W/H + 1.393 + 0.667 \ln(W/H + 1.444)]} \end{cases} \tag{25}$$

The above approximations using metallization profile T, static and relative permittivity ϵ_e and ϵ_r include the dispersion approximations $P(f)$ and $F(W/H)$ [40][42][43]. These values will be used for the transmission line (TL) model of Microstrip technology with classical distributed elements ($R_l, C_l, G_l,$ and L_l) (Figure 16). The linear resonator with equivalent length of $\lambda/2$ isolated (Q_0), near of the resonance the system is equivalent to a parallel RLC [16], resonance frequency given by (26), where n denotes the harmonic values of the fundamental value ($n = 1$) and v is the velocity of propagation in a substrate with characteristics ϵ_r and $\tan\delta$.

The distributed model allows to evaluate the influence of the coupling and express the resonator in a compact way to develop the future array of resonators. Resonance frequency depends of length of central line length l and the coupling feed lines.

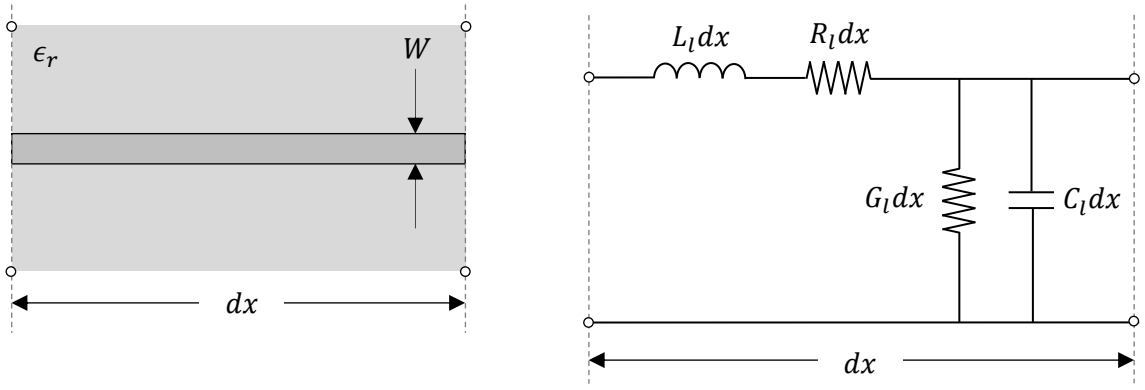

(a) (b)

Figure 16 *Lumped circuit model*. The TL is divided in infinitesimal values, where the voltage and current do not change substantially, the resistance per length (R_l), inductance per length (L_l), conductance per length (G_l) and capacitance per length (C_l) are characteristics of TL. (a) Infinitesimal transmission section and (b) lumped circuit distributed equivalence.

$$f_n = \frac{2v}{n\sqrt{\epsilon_{\text{eff}}}\lambda_0} \tag{26}$$

The selectivity of resonator is clearly related to quality factor Q_0 (17) and this, in turn, with the losses in the TL, the losses in Microstrip technology with the conditions of substrate, environment temperature and frequencies under 25 GHz mainly come from conductor (27) and secondly with the substrate losses (28). Certainly, the dielectric part does not depend directly on the frequency, although ϵ_{eff} is clearly a variable of the below of frequencies of 10 GHz.

$$\alpha_c = \frac{R_s}{Z_0 W}\left\{1 + \frac{2}{\pi}\tan^{-1}\left[1.4\left(\frac{\Delta}{R_s}\right)\right]\right\} \text{ Np/m} \tag{27}$$

$$\alpha_d = \frac{\mathrm{k}_0 \epsilon_\mathrm{r}(\epsilon_\mathrm{eff} - 1)\tan\delta}{2\sqrt{\epsilon_\mathrm{eff}}(\epsilon_\mathrm{r} - 1)} \text{ Np/m} \tag{28}$$

Where R_s represents the surface resistivity $R_s = \sqrt{\omega\mu_0/2\sigma}$, ϵ_eff is the effective dielectric constant of the planar microstrip structure and Δ is rugosity profile over conductor surface.

3.3. Model for Microstrip resonator

The selectivity of planar microwave resonator like an analogy of FBG technology used in the [10] is not comparable to the optical case, the losses inserted by the substrate and conductor limit the final performance of linear resonator. In fact, the Microwave case is only comparable by increasing the Q factor, decreasing the temperature (in order of 1.0 Kthus neglecting the conductive losses and the final Q_{ext} value could excess factors of 10^3. The above case recently have received a lot of interest like a method in circuit quantum computing and ESR [16][44]. For example, in spin electronic sensors the high selectivity of resonators allows to count electrons of order in 10^2 [45].

In microstrip technology a gap discontinuity is modeled by two capacitances (Figure 17) and the equivalent increase in length could be approximate by the expression (29), so the gap is

$$l_{eq} \approx \frac{cZ_0(C_1 + C_2)v}{\sqrt{\epsilon_\mathrm{eff}}} \tag{29}$$

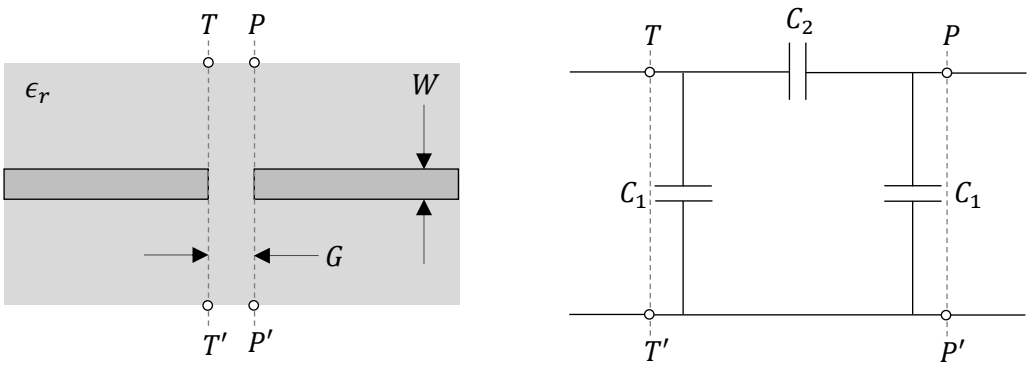

(a) (b)

Figure 17 *Gap in microstrip technology* (a) Symmetrical conductor lines and (b) C_1 correspond to end line with ground interaction (*TT*' with GND and *PP*' with GND) and C_2 is the capacitance between the two ends strips (planes *TT*' and *PP*') [25].

an important control of resonance frequency. The equivalent circuit has had high interest due to multiple applications mainly in filters design and quantum circuits. Another way to understand the behavior of the system is by considering that near of the resonance frequency the resonator behaves like a LCR circuit [44] so the quality internal factor of the resonator could be expressed by:

$$Q_{int} = R\sqrt{\frac{C}{L_n}} = \omega_n RC \tag{30}$$

Where the values for the equivalent LCR oscillator correspond to electrical distributed elements in microstrip technology (31) [46][47]. For a resonator isolated (30) would be the total quality factor, however, it required an injection of external energy and a coupling element to transfer such energy. In this case, the way is a gap or a capacitive coupling method, represented in the equivalent circuit (Figure 18) by C_κ.

$$L_n = \frac{2L_l l}{n^2\pi^2}; \quad C = \frac{C_l l}{2} \text{ and } \quad R = \frac{Z_0}{\alpha l} \tag{31}$$

An alternative for the circuit with coupling C_κ (Figure 18) is using an equivalent Norton circuit with the parameters (32) and (33) (Figure 19) [16]. Using this method allows expressing external and internal quality expressions in terms of known parameters. To describe the

incidence of capacitive values over final resonance frequency value, Q factor is directly related with losses (dielectric and conductor part) but the precision in the final resonance frequency depends on geometrical values and techniques of fabrication.

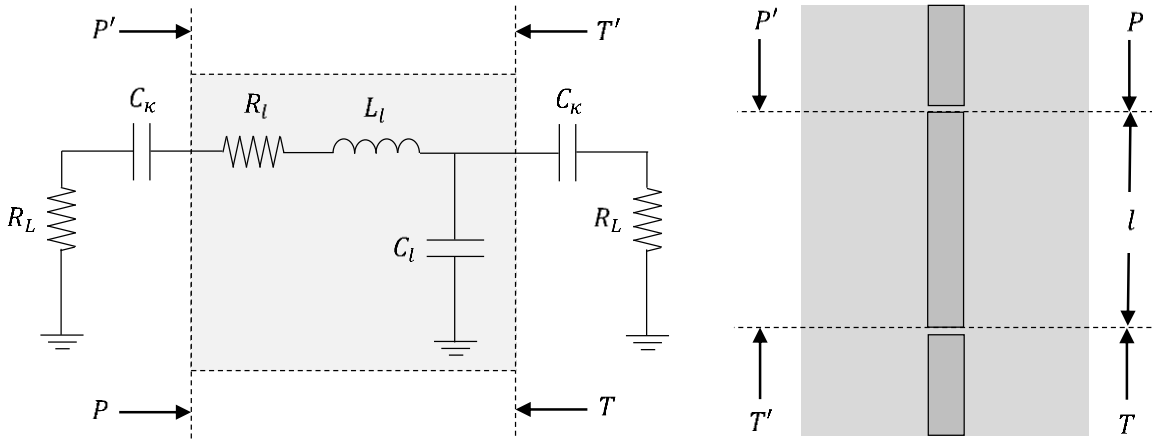

Figure 18 *Equivalent circuit (left) for λ/2 resonator geometry (right),* the proper values of R_l, C_l, L_l, C_κ and R_L are characteristics of design selected within the properties of material and external loads.

The circuit for the coupling capacitance and external impedance could change by a combination in parallel of resistance and capacitance. R_L is the external impedance of 50 Ohm, the conversion to R_N increase this value, which represent a decrease in the quality factor, however couple capacitance is the key on the final design [16]. Parameters are presented in (32) and (33), the new frequency is originally modified by the coupling method.

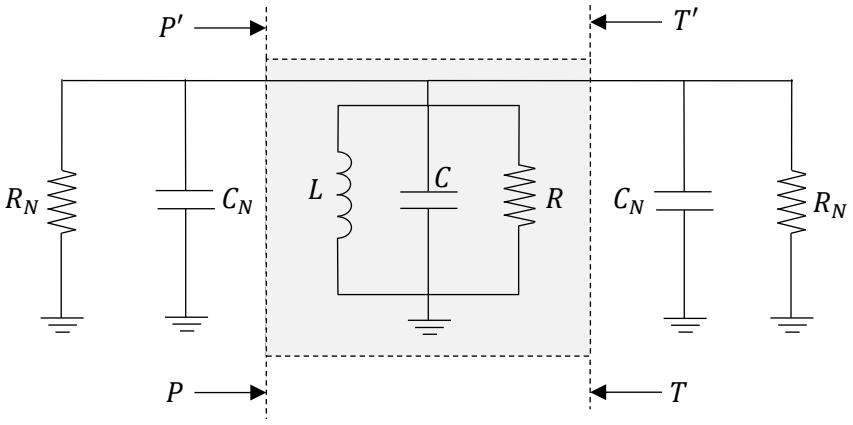

Figure 19 *Norton equivalent circuit* R_L and C_κ that represent the coupling of energy and external impedance are converted in two global variables

$$R_N = \frac{1 + \omega_n^2 C_\kappa^2 R_L^2}{\omega_n^2 C_\kappa^2 R_L} \tag{32}$$

$$C_N = \frac{C_\kappa}{1 + \omega_n^2 C_\kappa^2 R_L^2} \tag{33}$$

For the case of symmetrical feed lines of coupling, the load Q_L factor will be:

$$Q_L = \omega_n^N \frac{C + 2C_N}{1/R + 2/R_N} \approx \omega_n \frac{C}{1/R + 2/R_N} \tag{34}$$

Where ω_n^N is the new frequency of resonance shifted by the inclusion of C_κ

$$\frac{1}{Q_L} = \frac{1}{Q_{int}} + \frac{1}{Q_{ext}} \tag{35}$$

Using the physical parameters of design and expressions known for Microstrip technology [46][40][25], a linear resonator for 2.425 GHz using RO4350B and mechanical milling requires the following values of fabrication Lr $= \lambda/2 \ = \ 38.4\ mm$, W $= \ 1.23\ mm$ and G $= \ 0.25\ mm$. The behavior of coupling is analogue to a RLC circuit, the under coupling and over coupling effect represents the main effects of C_κ. The inclusion of Q_{ext} reduce the quality factor. Consequently, the selectivity of resonance, finally (35) produces the load factor quality (Figure 20).

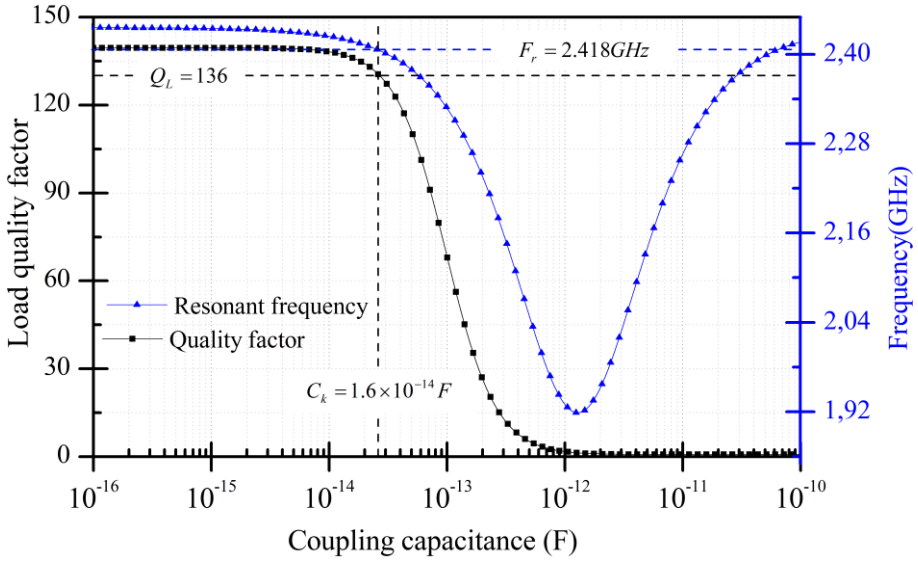

Figure 20 *Coupling effect.* The inclusion of capacitance coupling produces two main consequences; a frequency shifted and control of load quality factor, this last one is limited by material characteristics.

Using milling technique fabrication and VNA SOLT characterization, the results both in Q_L and resonant frequency are close to previous model Figure 21. The accuracy in frequency is around 0.5% (∼15 MHz), which according to precision of expressions for constitutive elements in Microstrip technology corresponds with the model. One way to increase quality values could require materials with high conductivities like superconducting devices or reduce $\tan\delta$, although the final value may be increased by a thousand factor, cooling methods and require precise lithographic processes, which is presented like a future research plan.

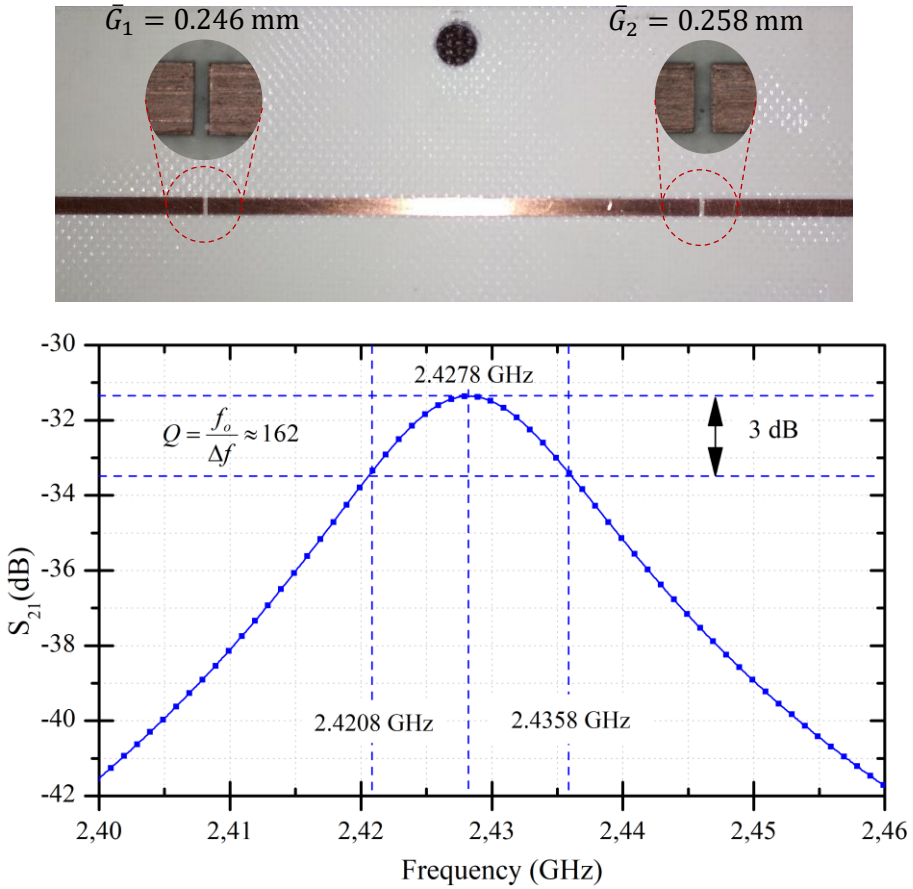

Figure 21 *Experimental S-band linear resonator* Experimental S-band linear resonator the model fabricated with mechanical milling and RO4350B substrate, the minimum bandwidth has gotten over this commercial material is around tens of MHz, requirements for frequency synthesizer similar to optical case it is no comparison because here the material includes losses limiting the final performance of the device. However, within the precision of fabrication and modelled system, the resonance frequency is within 0.5% of error.

The calculation of C_κ has been studied with certain limitations, the software's implementations is based on older references [48][49] with ranges of use limited by the W/H and

G/H ratios. Requirements in gap space are established at a maximum 300 μm, decreasing the distance between conductors increase the capacitance in consequence decrease the coupling factor, however, decreasing the capacitance implies rising the insertion loss in the system.

The linear resonator presents a set of harmonics (Figure 22), multiples of fundamental frequency f_0 or $\lambda/2$. The values for the subsequent frequencies are given by the expression (36).

$$f_n = nf_0; \quad \text{with} \quad n \in \mathbb{N} \tag{36}$$

With high values over n, the insertion loss is reduced against the reduction of the quality factor of the frequency considered.

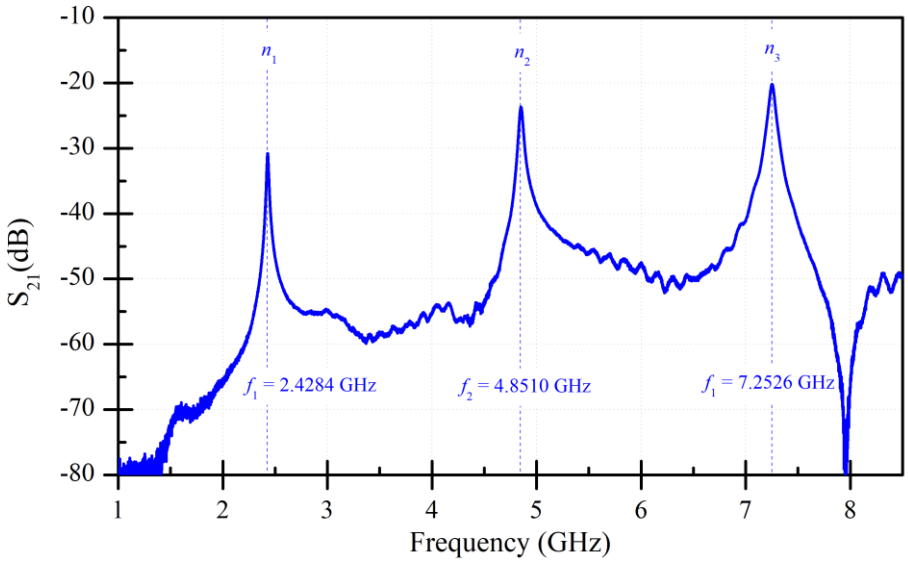

Figure 22 *Experimental response* Equivalent circuit (left) for $\lambda/2$ resonator geometry (right), the proper values of R_l, C_l, L_l, C_κ and R_L are adjusted with the real values, however the width of the conductor

The previous result shows loss insertion introduced in the design is in the order of 20 dB. The resonator circuit requires to increase the sensibility so it could be introduced by power amplifiers or active impedance transforming circuits [50]. Moreover, using these types of active elements improves the final selectivity of the resonator.

3.4. Summary

This section presented a close model of linear resonator using Microstrip technology, based on classical static approximations based on geometrical conditions, the close results found for the resonance and selectivity of system, require additional methods to get an approximate result in the frequency synthesizer. Finally, the coupling capacitance is a fundamental element to guarantee both the resonant and quality factor, with the help of expressions like (32) (33) (34) the process of design resonators are very close to the experimental case. The final precision with the design models presented here is around ± 10 MHz in the resonant final frequency.

Chapter IV

Methods

The frequency synthesizer design on Microwave Circuit technology requires some subsystems like the $\lambda/2$ resonator, the time delay section, impedance taper adapter and Wilkinson power divider. Each part is well known in Microwave technology, the material for manufacturing corresponds to RO4350B®, this material performed all the simulations and analysis, worth mention that EM simulations are as accurate as the substrate material specifications are given. Although the control of resonance and time delay with the requirements presented in chapters 2 and 3 is a tradeoff with material and environmental variables, the classic hybrid methods of fabrication, i.e.: Laser Ablation, Serigraphy and Mechanical Milling allow to get an approximation of the synthesizer proposed.

The chapter begins with a basic description of the FDTD method. It has a high interest in the recent years thanks to the increase of computational power and an attractive application as direct solution of Maxwell equations over time domain. For the process of coupling impedance together with simulations addressed in the previous section, allows to design and construct some probe resonators to check the resonance frequency and time delays. The method to measure time and frequency response of the system (DUT) is using standard VNA with TDR technique to check the time previously introduced.

For the Electromagnetic Computer Simulation, it was used XFdtd® (7.4.0.2) to test the spectral and time response.

4.1. FDTD method

The numerical methods to get approximated solutions of the Maxwell equations have been a hot topic in Electromagnetic and its applications field. Several approaches exist using rigorous methods, i.e., FDTD, FDFD, FEM or RCWA; crossing for full wave methods, i.e., MoM, BEM and BPM and finally scalar methods like Ray Tracing method. The mathematical formulation of FTDT is well known [26][27] since '60s, the Yee algorithm [51] and consecutively advances in computational power, attract the interest of multiple research areas which yielded the implementation in commercial software packages like XFdtd®, Lumerical®, OptiFDTD® and free packages like Meep [52].

The basis of the method is to approximate a function $f(x + \Delta x/2)$ using the derivative approximation (37) and $g(x)$ using the mean value between $x - \Delta x/2$ and $x + \Delta x/2$ (38). For the electromagnetic analogy $g(x)$ correspond to electric field $\vec{E}(\boldsymbol{r}, t)$ and $f(x)$ is the magnetic field $\vec{H}(\boldsymbol{r}, t)$.

$$f(x + \Delta x/2) \cong \frac{f(x + \Delta x) - f(x)}{\Delta x} \tag{37}$$

$$g(x) \cong \frac{g(x + \Delta x/2) - g(x - \Delta x/2)}{\Delta x} \tag{38}$$

For the case of lack of sources, the Faraday's law (39) and Ampere-Maxwell's law (40) will be discretized into the time domain by the following equations.

$$\nabla \times \vec{E}(r, t) \cong -\mu \frac{\vec{H}(r, t + \Delta t/2\,) - \vec{H}(r, t - \Delta t/2\,)}{\Delta t} \tag{39}$$

$$\nabla \times \vec{H}(r, t + \Delta t/2) \cong -\epsilon \frac{\vec{E}(r, t + \Delta t\,) - \vec{H}(r, t)}{\Delta t} \tag{40}$$

Clearly the electric field is computed in time steps different to the magnetic field, likewise in spatial case (Figure 23), but the Δt is the same. The philosophy behind is very simple, to excite the system with a known signal with the content of frequencies of interest, propagate this signal into the structure and solve (39) and (40) until electromagnetic energy will be dissipate by the system. Although FDTD method is very inefficient for highly resonant devices, this method is particularly useful to *hunt* the frequencies values.

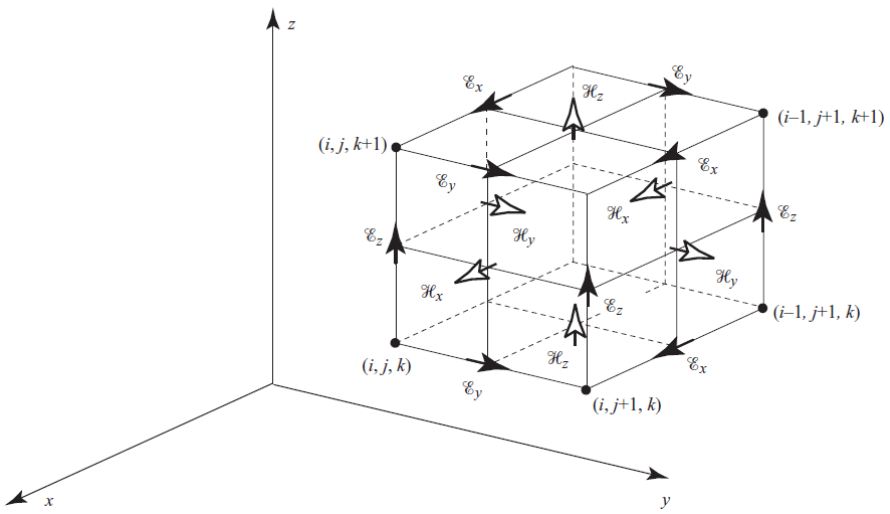

Figure 23 *Yee Cell for 3D case* the solution point for each case of vector field is different, this point selection allows to introduce the difference method to electromagnetic field (Image by [5 p. 73]).

To resolve the wavelength λ_0, the discretization using Yee cell requires a minimum N_λ elements per wavelength, this variable depends mostly on the type of material or application (41). Another element to considerer is the minimum distance or detail of structure $d_{\min}$ and divide this element by N_d which has a value depending of grade of detail of the system. The minimum between $\Delta_d = d_{\min}/N_d$ and Δ_λ produce the cell size required by the problem and the stability is guaranteed by Courant criterion selection for time step (42).

$$\Delta_\lambda = \frac{\lambda_0}{N_\lambda \sqrt{\epsilon_r}}; \tag{41}$$

$\boldsymbol{\Delta_\lambda}$	**Comments**
$10 - 20$	Low contrast dielectrics
$20 - 30$	High contrast dielectrics
$40 - 60$	Most metallic structures
$100 - 200$	Plasmonic devices

One of the advantages of the FDTD method is to directly get the input and output signal, for the case of transmission planar lines circuits is important to obtain the real behavior of the elements inside of the circuit. Clearly the computational requirements limit this method and for the resonator case the presence of the gap in the structure (Figure 17) impose the

$$\Delta t \leq \Delta t_{max} = \frac{\sqrt{\epsilon_r}}{c\sqrt{\frac{1}{(\Delta x)^2} + \frac{1}{(\Delta y)^2} + \frac{1}{(\Delta z)^2}}} \tag{42}$$

limitation that $G \ll \lambda_0$, the Courant stability factor required a small Δt, which implied a lot of computational time to the evolution of the system. Considering the narrow band to use in 2.4GHz with a RO4350B substrate ($\epsilon_r \approx 3.48 \pm 0.01$), λ_0 is in order of 30 mm and the gap in the resonators is around ~300 µm, so the gaussian pulse (Figure 24) require around one order of time more to propagate in the system [54].

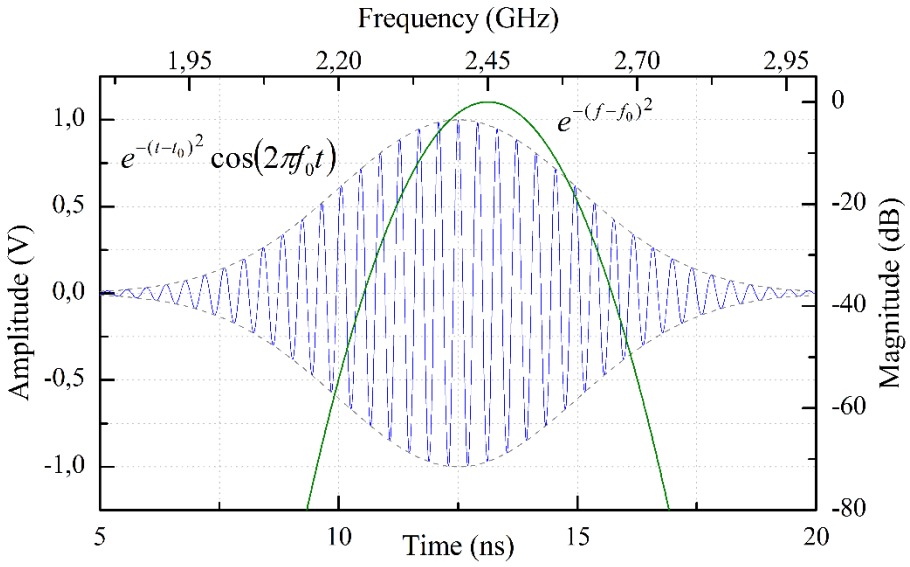

Figure 24 *Excitation function to the system on FDTD method* The interest band of frequencies for the actual design is the ISM 2.4GHz spectrum section, correspond to $2.4 - 2.5\ GHz$, incident power with narrow bandwidth is equivalent on time domain to gaussian modulated pulse.

Another concept to evaluate in EMC is the precision with the frequency domain, the FDTD method works directly on time domain so using the Fourier transform allows the system to calculate the behavior in frequency domain, the uncertainly principle implies increase the resolution in frequency increase the pulse time duration (Figure 24). High precision on frequency response requires a lot of simulation time.

To characterize the sample, the boundary conditions under FDTD method must reproduce the sample holder over the circuit is suspended. A complete enclosed metallic system in all directions (PEC in 6 boundaries) slightly modifies the impedance $Z_0 \pm \Delta Z$ [43] and makes possible to guide frequencies related with the geometrical of the holder. To minimize these propagation modes, Microstrip technology recommend a port minimum extension, however the presence of this peaks, only appears starting the second harmonics.

The samples holder used to characterize resonators were fabricated in two versions (Figure 25), simulations and experimental data obtained in both cases (Figure 26) demonstrate the presence of another frequency propagation modes, the precision between the 6 metallic boundary and the 3 metallic experimental conditions case respect to the main resonant multiple cases ($n = 1, 2, 3$) in equation (36), the presence does not change the main values. Within the three harmonic values, the difference is about $1 - 3$ MHz, so the inclusion of 3 additional bound walls increase the dispersion of the system but allows to hunt the frequency with the same range.

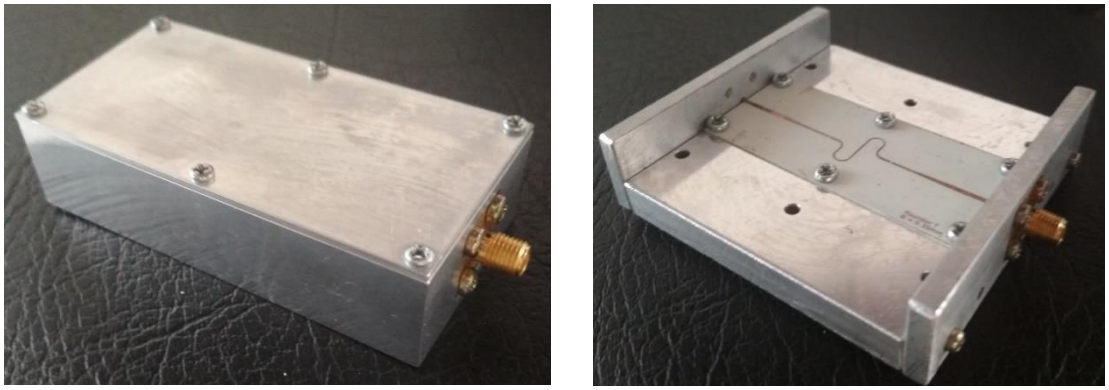

(a) (b)

Figure 25 *Sample Holder* (a) 6 PEC boundary conditions and (b) 3 PEC boundary conditions. The presence of frequencies not included in the harmonics of principal mode is a condition of propagation, the waveguide resulted in the presence of another frequencies

Another variable to extract on the simulation is the quality factor, FDTD use a profile gaussian signal, frequency precision is related with Δt and number of points [26][27][53], so the Fourier transform do not get near value of experimental Q_L (Table 3). Again, the peak location was well hunted, with a close resolution between simulation and experimental result,

Simulation XFdtd® (PEC on 3 boundaries/walls)		**Experimental frequencies (3 Aluminum walls)**		**Error**
Frequency	**Q_L**	**Frequency**	**Q_L**	**ϵ_f**
2.4236 GHz	107.2	2.4284 GHz	143.7	0.198 %
4.8358 GHz	214.9	4.8510 GHz	125.7	0.314 %
7.2367 GHz	313.3	7.2526 GHz	125	0.219 %

Table 3 *Resonant and quality factors* the differences between quality factors is provided by the constant interpretation of Fourier transform, the quality decrease with the number of harmonic frequency, the best Q is in the first resonant frequency mode [16].

clearly assuming some boundary conditions, reproducibility between case (a) and (b) in Figure 25 are shown in Figure 26, open metallic case present a better match between peaks (Table 3), metallic enclosed represent a challenge in terms on time simulation with the addition of three more peaks, however the multiples of main resonant frequency are matched with the simulation.

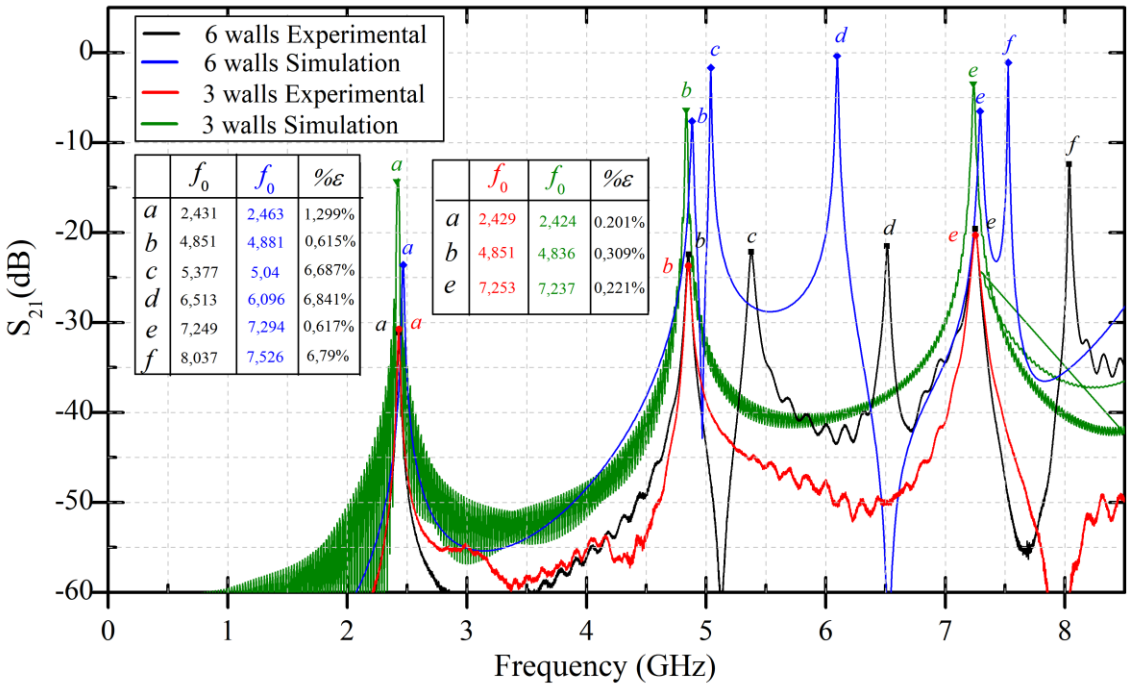

	f_0	f_0	%ε
a	2,431	2,463	1,299%
b	4,851	4,881	0,615%
c	5,377	5,04	6,687%
d	6,513	6,096	6,841%
e	7,249	7,294	0,617%
f	8,037	7,526	6,79%

	f_0	f_0	%ε
a	2,429	2,424	0.201%
b	4,851	4,836	0,309%
e	7,253	7,237	0,221%

Figure 26 *Boundary conditions*. The apparition of adjacent frequencies different to multiples of natural $\lambda/2$, correspond to propagation modes in the box of characterization. The metallic boundaries do not change the natural frequencies but add some new values, correspond to geometrical coupling with the metallic walls.

According to section 3.2, Q_L value agree on model included the losses characteristics, main limitation of FDTD method is in respect of above factor, but in relation of frequency peak is very correlated with the previous method and with the real measures. Some components are required for the final design in frequency synthesizer, the following section explores technologies used in Microstrip technology for the final design of frequency synthesizer. The parameter to check in the simulation will be used S-parameter measure by a VNA characterization.

4.2. Microwave Elements

To design and construct the synthesizer using passive elements it is required some elements to connect the pulse emitter to the RF detector using the array of resonators. The main two elements to analyze are: the power divider and the impedance adapter, to characterize the performance of both systems the scattering parameters S_{ij} will be get with the network analyzer ENA E5063A by Keysight® using OST method of calibration with the kit 85515A and TDR module analysis for the measure of time delay.

4.2.1. Network analysis

The standard calibration over the planes Port 1 and Port 2 (Figure 27) allows to reduce the systematic errors and unfold the behavior of the device (DUT). FBG works in reflective mode, related with S_{11} parameter, against the planar resonator in this study which is validated with the S_{21}. Both parameters relate amplitude and phase and characteristics of response for DUT, the condition in Port 1 and Port 2 is terminated in known impedance of $50\ \Omega$.

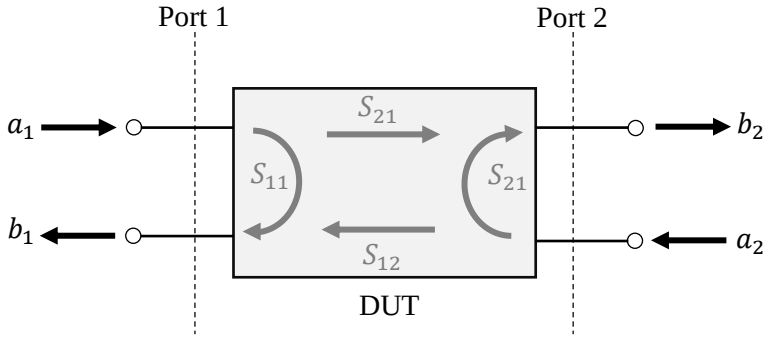

Figure 27 *Microwave 2-port calibration* Scattering method to characterize the device under test (DUT), *b* represents the wave leaving the device and *a* represents the wave entering to the system

The scattering matrix could be written by expression (43), the case of N −ports is easily generalized and used for power divider case of several ports.

$$\begin{pmatrix} b_1 \\ b_2 \end{pmatrix} = \begin{pmatrix} S_{11} & S_{12} \\ S_{21} & S_{22} \end{pmatrix} \begin{pmatrix} a_1 \\ a_2 \end{pmatrix} \tag{43}$$

Experimental setup presented for this research will be use the E5063A belong to Physics Laboratory of Electromagnetism in Universidad EAFIT, Medellín, Colombia (Figure 28)

and the N5241B in Laboratory of Electromagnetic Systems in IEAv, ITA, Brasil. The last one has a better performance in terms of dynamic range and frequency selectivity, calibration kit for this case was used the 85052D with 3.5mm connector, which outperform the SMA case in extended range. The local case has a difficulty in terms of using a converter connector, N type to SMA, plane of calibration is out of DUT and inclusion of degradation provided by the converter must be studied. It was compared the results between VNA in IEAv against the results of ENA case, presented a close results in terms of frequency and attenuation measures.

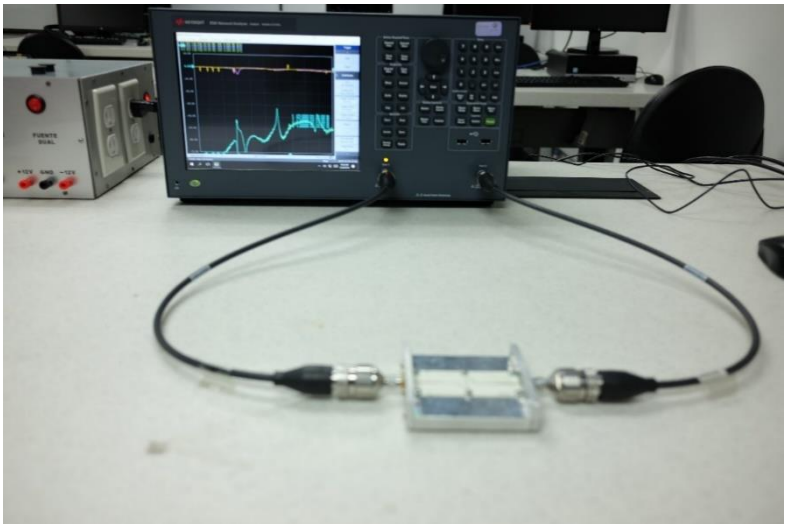

Figure 28 *Experimental setup* The VNA used was a E5063A with a 85515A OSLT mechanical calibration kit, although the calibration is not directly SMA, the insertion loss and VSWR included in the adapter was compared directly with the results of 3.5mm calibration kit 85052D.

Each resonator will be adapted to a power divider, a taper section and finally a delay line to simulate the random insertion time between adjacent symbols. This complete part will be discussed in section 5.3.

4.2.2. Wilkinson power divider

The section between resonator circuits and pulse emitter required equal power for each resonance symbol and isolation between adjacent lines, the Wilkinson divider is an option with good properties for insertion loss (IL), isolation and bandwidth (BW) [39]. Ideally, the power

is equally distributed into N ports, to 4 ports -6 dB is the output on each port, another two parameters to analyze are the isolation analysis between output ports and bandwidth.

To test the requirement on Port 1,2,3 and 4 (Figure 29b), simulation displayed is according with the requirements on array element, limitation on the bandwidth and necessity of another passive element is a condition for the development of this type of element, however all the

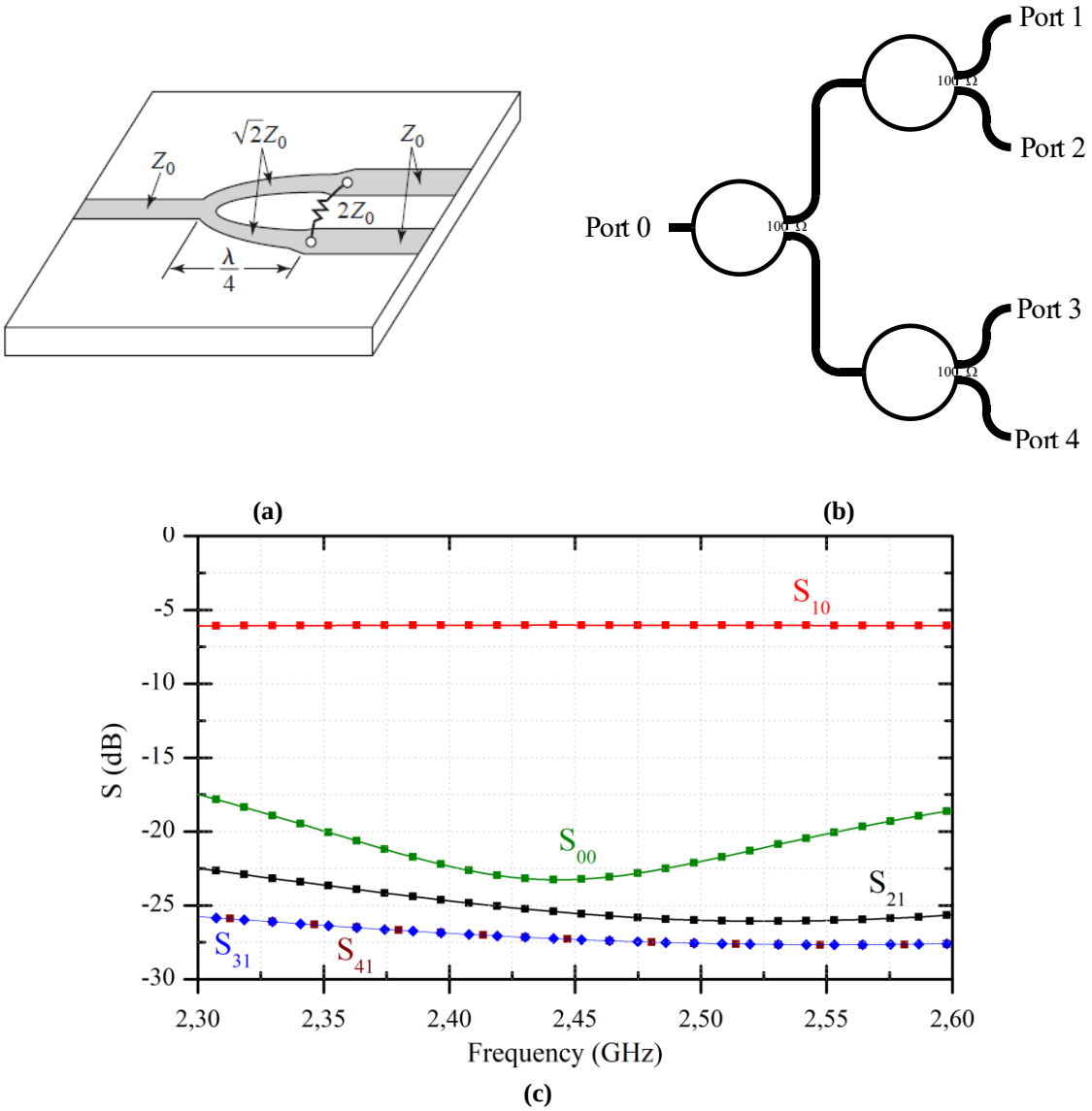

Figure 29 *Wilkinson power divider* (a) This passive structure is based on $\lambda/4$ for $\sqrt{2}Z_0$ within a bandwidth the directivity is enough for this application Image taken from [39] (b) Resonators array were designed for codes $\mathcal{H} = \{13, 4, 0, 4\ mm, 1, 0\}$ (sec. 1.4), system with four output independent ports and (c) XFdtd® simulation shown a isolation under $-20\ dB$ which is taken for reference into the design of microwave devices, the bandwidth cover the S region spectrum for ISM and equal power is shown for each resonator arm, around $-6dBm$.

ports are matched and outputs are kept isolated.

The frequency band proposed (ISM 2.4GHz) has a central value of $f_0 = 2.445$ GHz with a bandwidth nearly to 100 MHz, the main idea is behind to IEEE 802.11b standard, which use DSSS in physical layer with 13 channels divided by 22 MHz between adjacent channels. The three treat-offs to balance the performance of power divider are based in insertion loss, isolation between ports and bandwidth. The selection of material was imposed by the stability of dielectric constant ± 0.05 for RO4035B material [23]. The main losses in Microstrip case are provided by conductor part (section 3.4).

4.2.3. Exponential Taper design

Inclusion of taper or impedance transformation is a requirement for reduce space and control capacitance coupling factor, this is possible to reduce the width of the conductor decreasing the gap with the consequence of reduce insertion loss. Using RO4350B, the taper covers changes from $50\ \Omega$ up to $90\ \Omega$, limitation is mainly the process of fabrication, i.e. with a board of $\mathrm{H} = 0.508\ mm$ in height, the widths of conductor for $Z > 90\Omega$ required conductors of $400\ \mu m$ [40] which are achievement using lithography techniques, with mechanical and xerography is possible but reduce the reproducibility of synthesizer system using only passive elements.

The final section allows to control of coupling capacitance C_k, finally the quality factor Q_L is controllable with the gap geometry distance. Although the exponential case is no optimized in terms of length and Γ coefficient, it is easily to implement and to control in terms of impedance for Microstrip technology. The profile of impedance is given by expression (44):

$$Z(z) = Z_0 e^{az}, \quad 0 < z < L \tag{44}$$

Where L correspond to length of taper line and the constant a es given by the expression:

$$a = \frac{1}{L} \ln\left(\frac{Z_L}{Z_0}\right) \tag{45}$$

The characteristic impedance here is $Z_0 = 50\ \Omega$ and $Z_L = 90\ \Omega$, the length of taper require a value with $L > \lambda/2$ at expenses of increasing the reflection coefficient. Construction and

characteristics of taper are displayed in Figure 30, the taper section matched with the simulation in time domain, there are variations on the impedance values, mainly from fabrication method, differences in width conductor produce important changes over the impedance final value, changes of 10 μm could increase the impedance in units of Ohms. The value of 90 Ω is close to 80 Ω around of 60 μm of difference, which correspond with tolerance in method of fabrication and design.

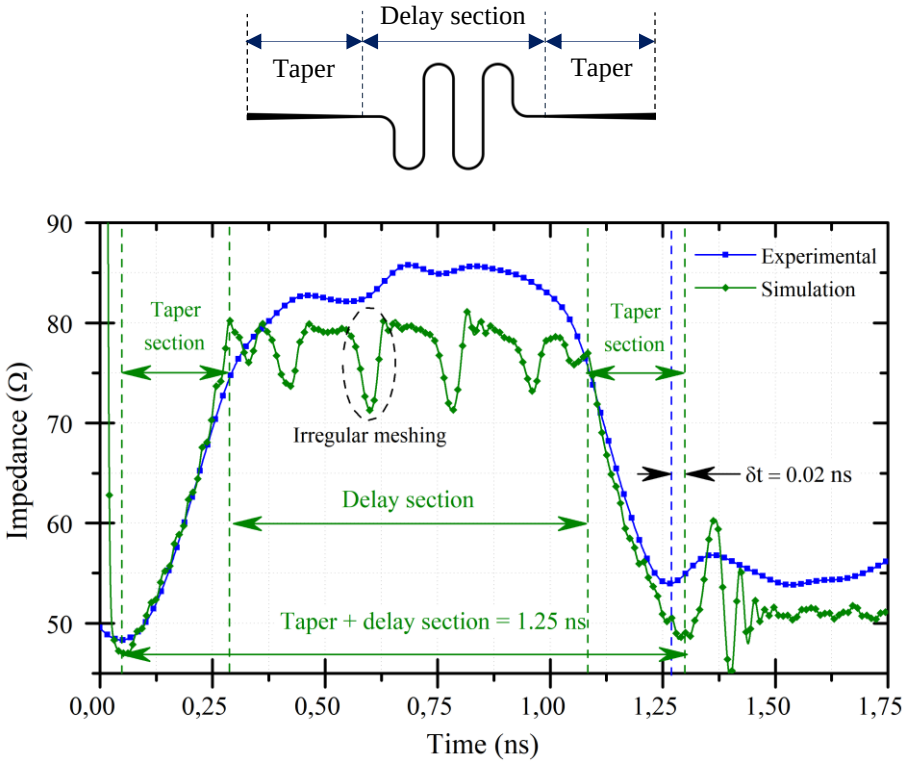

Figure 30 *Exponential taper and time delay section* Implementation of taper section is according to results of simulation, the time difference between both models is around 20ps (near of the limits of TDR module (46)), the oscillation on TDR signal for the FDTD method is proper staircase of the curve shape.

Z_L is the final impedance coupling design, for this case it was selected 90 Ω like final value, foreseeing the limitation in fabrication method, the main criteria is Q final factor and the gap dimension to reduce the insertion loss but using only transmission lines is very limited. Two of the major limiting parts are the use of copper and substrate with $\tan\delta > 10^{-3}$, however a factor of 200 is enough for this application, the main limitations will explore in section 5.

4.2.4. Time delay insertion

To include the fabrication techniques and board material, the Microwave industry has a well-developed protocols and standards to introduce the variations of simulations against the fabrication methods. TDR belongs to these methods, using structures like series and parallel resonators, Beatty Standard, SOLT calibration, MBM de-embedding process and so on. It allows to directly test the performance of the fabrication process and material stability [55].

The behind selection of microstrip technology like method of fabrication is based on the idea that introducing a time delay τ_d is directly and unique associated with the conducting line extension and effective constant of substrate (24) [56]. Using this value for relative constant, the time insertion delay could be expressed by:

$$\tau_d[\mathrm{s/m}] = \sqrt{\mu_0 \epsilon_0 \epsilon_{eff}} \tag{46}$$

The minimum value of spatial resolution in TDR technique are limited by the rise time, T_r, or directly the bandwidth of the device, the minimum distance resolution is given by (47)

$$L_{min} = \frac{T_r c_0}{2\sqrt{\varepsilon_r}} \tag{47}$$

The TDR module on ENA5063A has a bandwidth up to 18 GHz with 24.8 ps of rise time, minimum distance resolution considering (47) and RO4350B characteristics is around 2 mm. For example, the meander delay section presented in Figure 30 introduce a physical equivalent extension presented in Table 4.

	Design [mm]	**Experimental [ns]**
Equivalent length [mm]	50.672	0.799

Table 4 *Insertion delay comparison.* Using expression (46) and $\epsilon_r = 3.48 \pm 0.05$, the calculation for time insertion delay is 0.269 ns.

Likewise, implementation requires geometrical paths with spectral properties for the frequency band selected, the meander case is a well-known structure with spectral response easily to control [10]. The taper section in Figure 30 clearly do not present a minimum value for exponential case, $\lambda/2$ [39], degradation in frequency is evident in terms of S_{11} displayed in Figure 31. Although the region of interest is on the left of the design, $-10\ dB$ is a good

tradeoff for the combinations Taper plus delay for board characteristics and selectivity requirements.

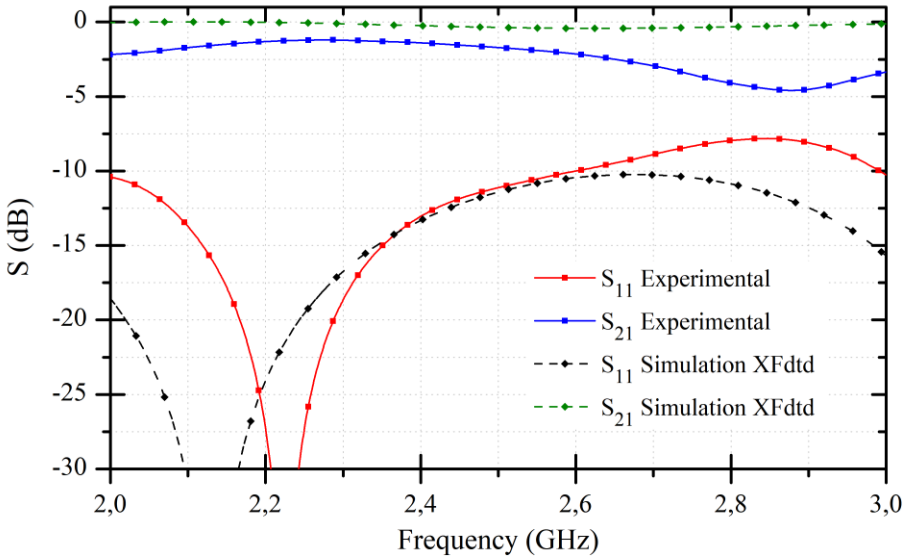

Figure 31 *Frequency response to time delay and exponential taper* The response in time domain was presented in Figure 30, efficient operation range is nearly of 2.4 GHz, extension of exponential taper reduced the value of S_{11}, practical requirements is based on $-20\ dB$ for reflecting power.

4.4. Summary

Microstrip technology has excellent correlation between design, performance, easy control of impedance and time delay dependency with conductor length. The results displayed for FDTD method certainly match with the frequency, time domain, so the election of this method guarantee the design process, only limitation is computing time. Again, precise resonance or delays sections parts require fabrication methods with good agreement between design and results, selection of material fulfillment requirements to selectivity and performance for final synthesizer.

Chapter V

Results

Resonators studied previously on time and frequency domain and time delays insertion allow to introduce the process of coupling several symbols (frequency carriers) and test the frequency synthesizer idea. The results on previous chapter, about resonance frequency and time delays using standard methods in Microwave Technology; VNA scattering coefficients and TDR technique, produced a high reliability against the simulation proposed. Errors near of 1% (Although these relations are a static approximation within 0.6% [41]) are closed to tolerances in fabrication process, so the meshing requirements of simulation process are enough with plasmonic applications (41).

Array of resonators is based on family $\mathcal{H} = \{13, 4, dl, 1, 0\}$, the space between adjacent symbols is correlated with random insertion time explored in sec 1.3. The design of the circuit and geometrical elements were developed in free software Inkscape®, mechanical milling and Serigraphy are used like approximation methods for construction of resonators. However, it will show serious difficulties in terms of replicability and reliable in an array which depends of precise dimensions for specific resonance frequencies and precise time delays.

Initially it will be presented the inclusion of time delays as the consistency with the frequency response, then it is detailed the resonator response and finally the synthesizer transceiver design and performance are presented. It will be compared with the previous results in OCDMA using FBG and proceed to evaluate the BER and performance of the communication.

5.1 Time delay introduction

The insertion of gaussian pulse in FDTD method produce directly the power behavior over circuit (Figure 32), which for correlation detection case is required, on the other side method require a high computing supplies to get a reasonable result (-30 dB of difference) and structures with resonances increase the time even more, the main reason behind is to dissipate all the input power into the system, high Q values requires high computing times.

Another important variable is the output power in terms of time, profile in case of FBG poses some close relation with the power output of resonators with condition of high Q value, again the idea is to find the response on time and spectral domain, final response of the cross correlation synthesizer requires of both values.

Firstly, time delay introduces spectral dispersion (Figure 32). The peaks in the graph contain many frequencies and taper exponential section was designed for S band, so the peak is expanded on the time domain, reflecting frequency components included in broadband peak used for XFdtd® to solve the problem, there are two possible approaches to simulation in FDTD, selecting a broadband range with a sequent filters bank or on the another way using

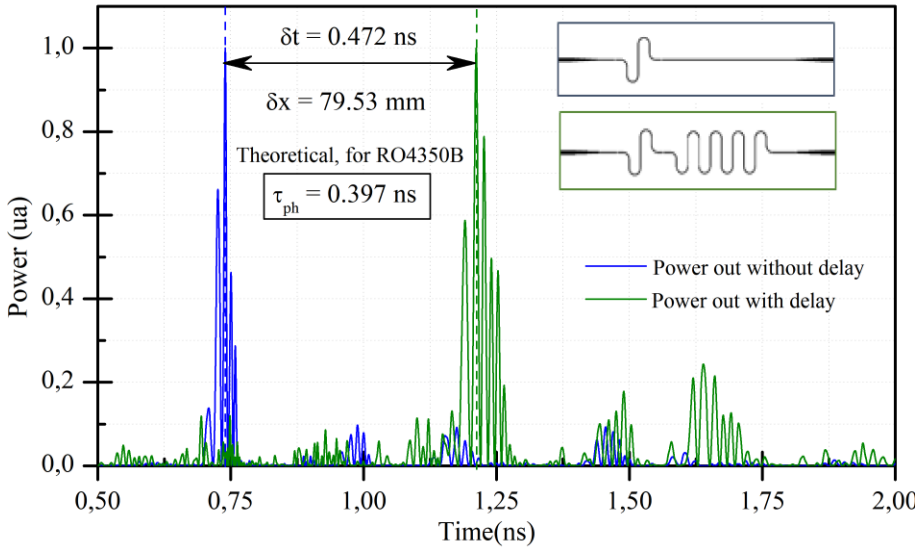

Figure 32 *Verification of time delay insertion* the difference between the simulation and expected value is around 70 ps, meshing the curvature structure of meander is a severe difficulty for the FDTD, to reach the closest value of time delay required a very fine meshing. The different shapes of the wave function are due to inclusion of delay which introduces some additional frequency dispersion (Figure 31).

narrow band, with allow introduce only the precise band; using the first methodology lets to explore interactions with dispersive material.

Response on time domain is according with the calculation in expression (46), the difference is about 70 ps, staircase phenomena was observed in Figure 30 with the strong dependences to the value of impedance, this is a very weak difficulty over FDTD method applied over curvature structures.

5.2. Meander resonator

Resonator using meander geometry requires a meshing with high density of elements, i.e. extensive computing time, using conformal techniques could improve the time and memory resources required [57][54], however . Staircase over curves surfaces introduce errors over the equivalent length of resonator, but the simulation clearly has a trending behavior (Figure 33) to resonant value (~0.6 %) and insertion loss, the only aspect to considerer is the BW. For FDTD method, Fourier Transform $\mathcal{F}(\omega)$ increase the precision over ω at expenses to increasing the time observation, to improve the results over meshing cases below, it is required a high-density meshing computing time.

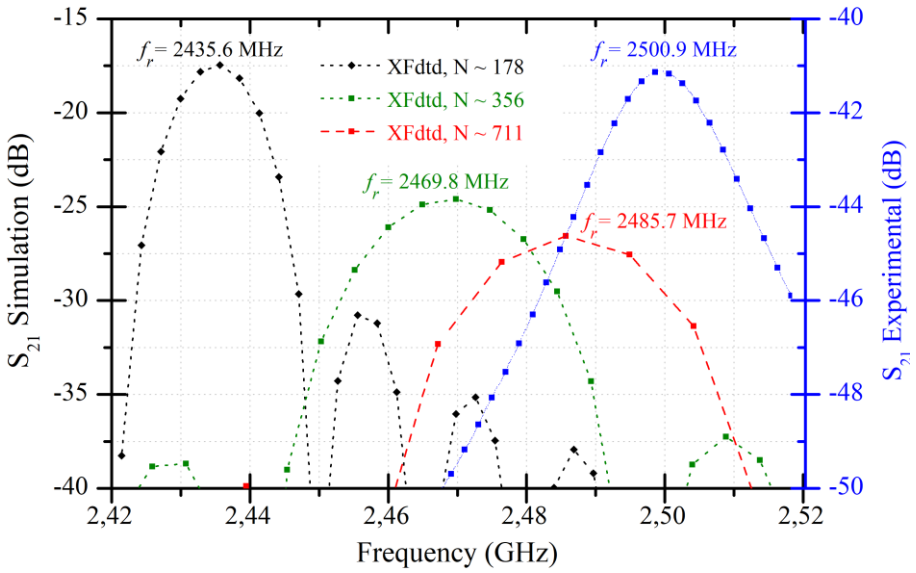

Figure 33 *Characterization of Meander Resonator*, using FDTD and Experimental data, the trend of meshing is 2502.8 MHz, which generates a error or 0.1%, but required a meshing with number of element per wavelength (N) in order of thousand. With 700 elements per wavelength the error is near to 0.7%, enough if is considered the error insertions due to fabrication and characterization process.

The time insertion response in Figure 32 is not the output response for S band range of frequencies, in fact for central case $f_c = 2.450$ GHz propagation on board material RO4350B ($\epsilon_{eff} \approx 2.54$), requires at least 400 ps to produce a complete oscillation. However, the complete power output presented below (Figure 34) include high energy components outside of S band, in fact, the main resonance of the system is directly in λ or $2f_0$.

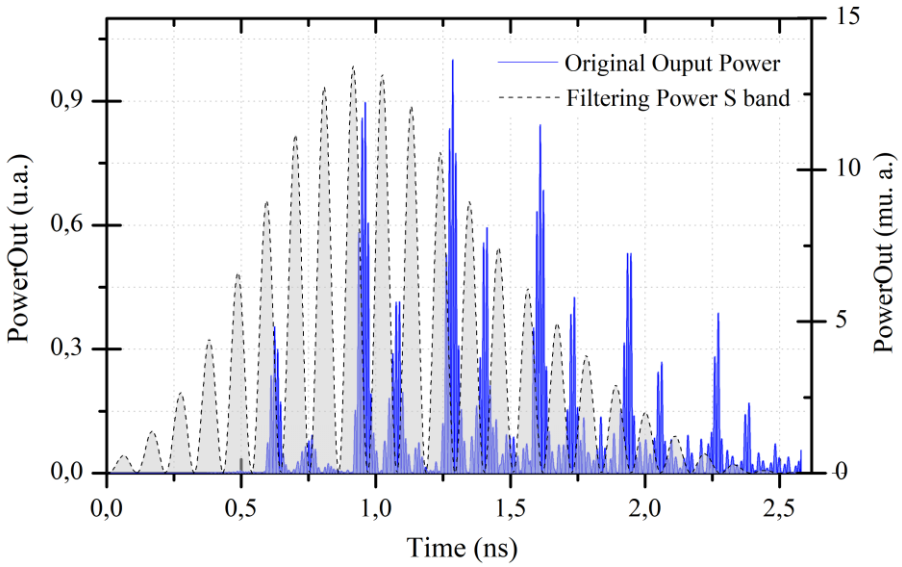

Figure 34 *Spectral pulse composition* Complete Gaussian pulse excite all possible frequencies on the meshing. This exceeds the narrow band analyzed in the present study, insertion of digital filter system for S band produces the well-known modulated Gaussian profile, modulated signal corresponds to power behavior.

The data presented above show the energy composition for S band, right axis confirms two magnitude orders of difference between S band high power peaks, Gaussian modulate pulse energy occupied around 2.0 ns, to reproduce the similar case presented in [10] physical separation between spectral components must be this value.

Assuming a log normal power distribution (Figure 35), ISM S-band region was divided in $q = 13$ symbols, BW got it with TL resonators is near of 100 so minimum restriction for separation $d = 4$ produce a code with $L = 4$. The carriers are $f_n = 2396.15 + 0.1n/13$ with $n \in \mathbb{N}$, each encoding symbol produce a power output increasing the sidelobes of cross correlation function, expressed in mean power values by the below figure. For log normal distribution, 80% of main power is in the interval $\mu \pm 4\sigma$, so the pulse will be considered of 1.5 ns duration.

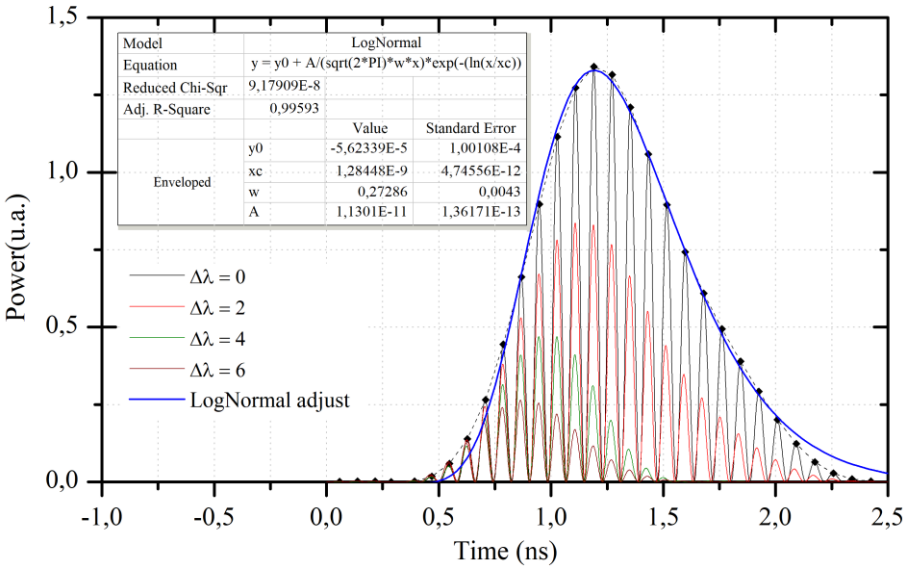

Figure 35 *Resonator Spectral Response*. Power profile outgoing of each the resonator (symbol) will be define with spectral distance. Low Q values in narrow band symbols imply high cross correlation energy.

5.3. Frequency Synthesizer proposed

Array of resonators in Microwave region is a hot current researching area with applications like, antennas arrays and metamaterials, pulsed ESR to generate homogenous in plane magnetic field [58], sensing capabilities in MKID [59][60][61], plasma generation [62], quantum computing architectures [63], Microwave SQUID Multiplexing [64][65] and so on. The design proposed here is limited by lossy material characteristics (RO4350B) in consequence the quality factor around 200 limited bandwidths of resonators, which theoretically is at maximum some tenths of MHz

The idea is to test the inclusion of time delays in consecutive resonant structures, the system is composed by Wilkinson power dividers (4.2.1), taper sections increasing impedance (4.2.2) and controlling coupling capacitance, posterior to each resonant case it is introduce time delays (Figure 36). Testing family generator is $\mathrm{G}_0 = (5, 6, 8, 7)$ in agreement with section 2, Bin algorithm [1] produce $q = 13$ codes using the recurrent way (48):

$$C_n = (5 + n, 11 + n, 6 + n, 0 + n) \ (\mathrm{mod}\ q), n \in \mathbb{N} \qquad (48)$$

Adjacent symbols within codes avoid the lateral lobules in auto correlation function, which is an important parameter to improve in orthogonal codes, however two consecutives codes,

C_n and C_{n+1} are only separated $\Delta\lambda = 1$ in adjacent components, with spectral response presented in Figure 35, interference provided by users with similar codes (close values for n), produce a high power values over the cross correlation function, for example, codes with $\Delta\lambda = 1$ impact with power distribution of almost 50% of central auto correlation peak value.

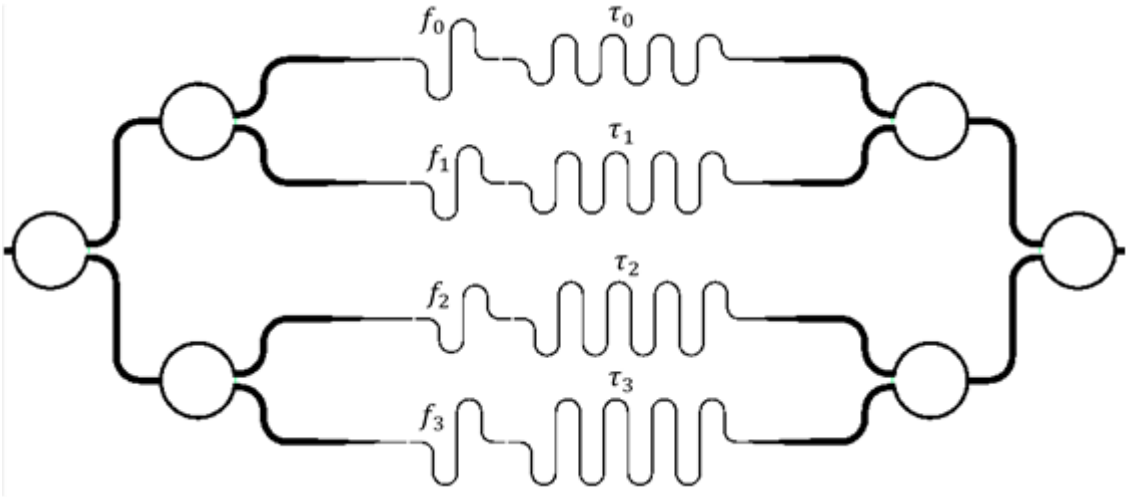

Figure 36 *Frequency Synthesizer proposed* using microstrip technology, the time delay is easily controllable, the value is only function of conductor length, although increase the length is equivalent to increase the loss in transmission, the receiver section is just the opposite case, the final loss in each frequency is the same, at least in terms of losses for metallic conduction.

Time delays τ_i insertion must support and spread the cross-correlation peaks, Hamming spectral function $\Delta\lambda(X, Y)$ detects the difference between each cell (Figure 37) and profile of power response for each case $P(n, \Delta\lambda)$ (Figure 35) is added. Intensity over the detector could be expressed by the following expression:

$$I(t = \varphi) = \sum_{n=0}^{NL+K} P\left(n, \Delta\lambda\big(X(n), Y(n+\varphi)\big)\right), \quad 0 \leq \varphi \leq NL + K \tag{49}$$

Where L is the length of the code, K is the total delays value, T is the sampling time and $I(\varphi)$ is the cross-correlation value. Each new value for $I(nT)$ require a shift over user code, there are some regions of code with null energy over the cross-correlation functions (shadow regions in Figure 37). To decrease cross correlation the next time step $(n + 1)T$, the system needs to increase the shadow regions. This implies to distribute randomly time between each

frequency symbol, but each user needs to assign different values, so the problem is equivalent to produce different ways to sum a natural number in a different ways, this type of requirements is named partitions functions [33].

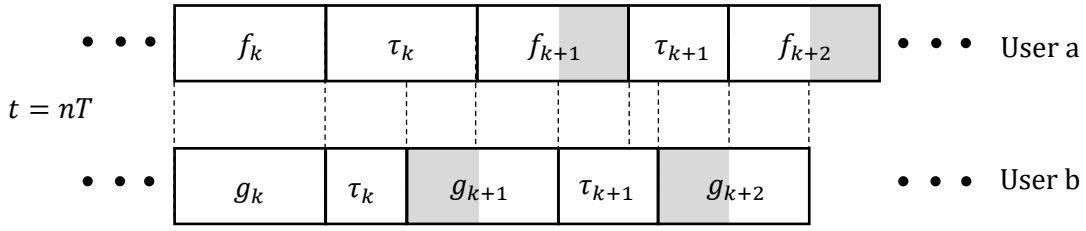

Figure 37 *Cross Correlation on time domain.* At time $t = nT$, superposition of both codes generates an output power based on spectral separation.

Using the uniform separation autocorrelation function has a significant peak in central case (Figure 38a), however there are sidelobes even without interferers absence, clearly spectral response and crowded carriers in a narrow band present a major probability collision event. The scenario with 3 users without time separation (Figure 38b) produce false detection, in

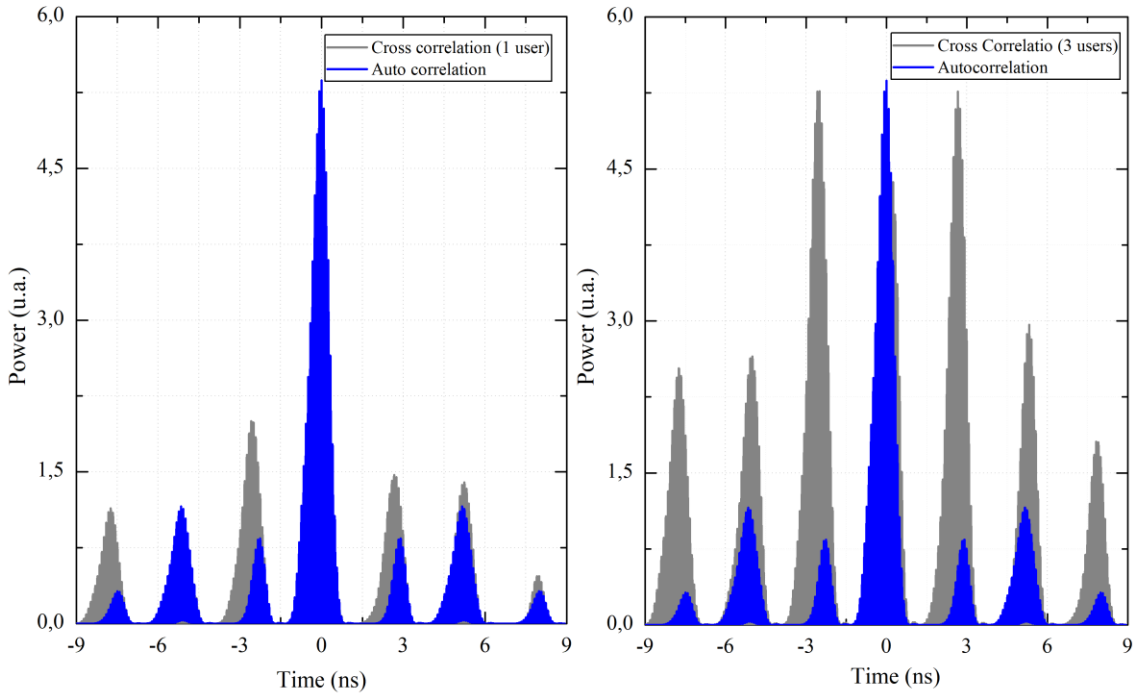

Figure 38 *Cross correlation synthesizer* time scale compared to Figure 11, spectral response for S band resonators implemented has a response with 3 shared users generating conflicted cross correlation adjacent peaks, in fact only 3 users over the channel generate enough interference to produce same probability in bit detected.

fact, sidelobes are equal to autocorrelation central value. Introducing time delays between adjacent symbols like original research [10], but again sidelobes has an significant event against identification of central power peak.

In Figure 11 it was presented FBG array with separation of 40% related to time duration of pulse output, RF case use around 400ps of free separation between adjacent symbols, again the cross correlation pulses increase power with increase the number of users (Figure 39a-b). The codes C_i and random times spaces M_{τ_i}[ps] (50) assigned to each user are presented below, calculating the cross correlation profile with (49) and with spectral characteristics founded for microstrip resonators, the peaks sidelobes are notorious reduced (Figure 39).

$$C_i = \begin{vmatrix} 5 & 11 & 6 & 0 \\ 6 & 12 & 7 & 1 \\ 7 & 0 & 8 & 2 \\ 8 & 1 & 9 & 3 \\ 9 & 2 & 10 & 4 \\ 10 & 3 & 11 & 5 \\ 11 & 4 & 12 & 6 \\ 12 & 5 & 0 & 7 \\ 0 & 6 & 1 & 8 \\ 1 & 7 & 2 & 9 \\ 2 & 8 & 3 & 10 \\ 3 & 9 & 4 & 11 \\ 4 & 10 & 5 & 12 \end{vmatrix} \qquad M_{\tau_i} = \begin{vmatrix} 69 & 80 & 1051 \\ 343 & 768 & 89 \\ 217 & 218 & 765 \\ 432 & 567 & 201 \\ 404 & 738 & 58 \\ 311 & 822 & 67 \\ 88 & 1108 & 4 \\ 281 & 440 & 479 \\ 173 & 452 & 575 \\ 368 & 769 & 63 \\ 39 & 159 & 1002 \\ 248 & 397 & 555 \\ 267 & 811 & 122 \end{vmatrix} \tag{50}$$

Again, only using blank separation improve the median of power signal reducing σ_I^2 on the detector and could BER quality measure improve, however the adjacent peaks in the cross correlation increase with the user number. Uniform time delays produce coincident times spaces where user cross correlation (Figure 39ab) peaks increase the value. Introducing ran-

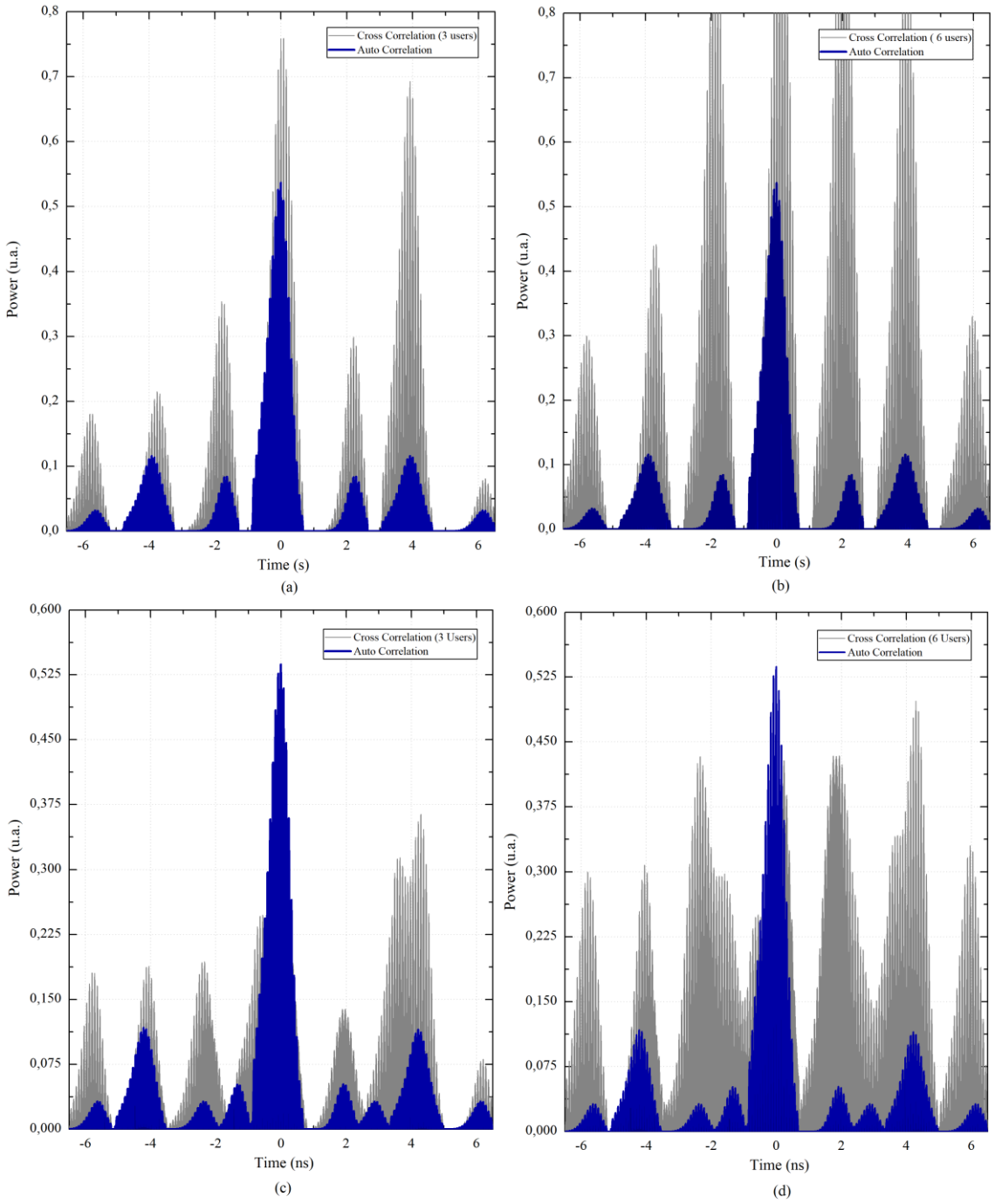

Figure 39 *Random Separation.* The frequency synthesizer displayed beneath using family generator $G_0 = (5, 6, 8, 7)$ adding uniform separation of 400ps between each encoding frequency with (a) 3 interferes and (b) 6 interferers, distributed this time separation randomly (c) 3 interferers and (d) 6 interferers. Distribution of time delays reduce significantly sidelobes, however the auto correlation sidelobes produce interference due spectral response of the system.

dom time delays try to use this time spaces to reduce the coincident adjacent peaks and spread this power values, although median and variance in time domain does not improve, the dynamic range in decoding system is increasing, with 6 users and trade off in spectral design for encoding part, the synthesizer produce (Figure 39c-d) a clear distinction between users, central peak of autocorrelation is more energetic than cross correlation counterparts.

5.4. Summary

The inclusion of random time delays improves the cross-correlation function generating sidelobes energy peaks decrease. Design of frequency synthesizer using the resonators designed in previous chapters, even with the low values of quality factor fabricated could be used to test the protocol but the main limitation is the precision in the technique.

Conclusions

Insertion of random spaces using a partition approach reduces the sidelobes in cross correlation function for the frequency synthesizer proposed. Dynamic range for SCDMA is improved and capacity of network in terms of user number enhance to tolerate high values of MAI caused by active users in the network. Cardinality on family in OC1d limits user number, but with the full network active, the interference reduces traffic at levels of DS3. The analog method proposed here improves significantly optical and Microwave synthesizer designed and analyzed previously.

Coupling case of FBG and exploring random spaces in Figure 9 showed insertion time delays proposed by [24]. It could be extrapolated to delay times into SFH-CDMA case with RF encoding-decoding system using linear resonators and controlling the time delays equivalently with delay lines in Microstrip Technology. Q factor for Microwave case studied previously is limited by conductor and substrate losses. However, the results in Figure 39 and Figure 10 showed spreading lateral peaks power using random approach, allowing to study even with low quality resonators.

The simulation of coupling several symbols (frequency carriers) got it in the previous section (sec. 5) allows to test the RF synthesizers idea using linear resonators, power dividers, tapers, and delays sections, checking the frequency and time performance. Encoding system proposed for frequency synthesizer was detailed to determine the encoding-decoding system. It was exposed the insertion using partitions function for time delays section. FDTD method in XFdtd®, although requires high computing times and robust hardware requirements, presented a good balance between simulation performance and experimental results.

Random approach using partitions to get M_{τ_i} is an agile method to find time delays with the properties to avoid coincident lateral peaks in all the cross correlation cases. However, it is required a deep search to understand which are the better time distribution limits and searching methods to produce these delays. The random time distribution improves the access method to channel using correlation detection in SCDMA. Applications of this method could

be in car navigation radars [66] where the interference and hardware is fixed. For the digital case, switching time is the main bottleneck and delay times must be multiples of the clock system.

Microstrip Technology using manual screen printing and mechanical milling fabrication using commercial R0450B material is a tradeoff method to produce accurate geometrical dimensions of circuit. However, for microstrip technology using static approximation expressions [42][40] produces a 0.5% standard error and commercial software uses this approximation to design. This error of 0.5% in frequency domain is equivalent to 10MHz in symbol carrier. To improve this approximation, it is required precision on the geometrical dimensions, only possible with optical approach like lithography techniques.

Different families of OC1d produce a slightly different performance over the correlation synthesizer. The family set of generators were characterized in terms of BER performance for correlation detector, so the algorithm of generators produces families with different performance. Selection of families $\mathcal{H} = \{13, 4, dl, 1, 0\}$ and $\mathcal{H} = \{29, 8, dl, 1, 0\}$ allows to analyze all the generators using Bin [1] algorithm. In this sense, mathematical properties seem the same from the point of view of generation, but results in term of BER indicate a slightly structure of this generators over the correlator detector.

Future works

Manual fabrication like local screen printing or silkscreen is a testing process for RF fabrication circuits with limitation in high precision requirements. Lithography is a next approach to fabrication of this type of resonators array. The application is not only in communications protocols; high Q resonators have had an increasing interest in multiple fields where the models and test protocols developed in this research contains the start points to posterior implementations.

Clearly, the material and method of characterization limits the resolution over time random spread capacity and frequency selectivity. Division of 2.4GHz ISM band in 11 symbols require Q factors in order of 150. This is not problem with the techniques and material presented in this research, but the reproducibility of each symbol depends on accurate methods of fabrication. So, to introduce a real application, it is required an accurate method of fabrication based in passive elements, adequate for a crescent microwave industry.

High correlation between models and FDTD simulation could improve the frequency values, extending the time and computer capacities (Figure 33). One of the difficulties is about curve structures; meshing requirements presented to improve the precision requires an extensive computing time.

References

[1] L. Bin, “One-coincidence Sequences With Specified Distance Between Adjacent Symbols For Frequency-hopping,” *IEEE Trans. Commun.*, vol. 45, no. 4, pp. 408–410, 1997.

[2] D. Torrieri, “Frequency-Hopping Systems BT - Principles of Spread-Spectrum Communication Systems,” D. Torrieri, Ed. New York, NY: Springer New York, 2011, pp. 159–212.

[3] H.-J. Zepernick and A. Finger, “Applications of Pseudo Random Signal Processing,” *Pseudo Random Signal Processing*. pp. 225–389, 07-Nov-2005.

[4] E. H. Dinan and B. Jabbari, “Spreading codes for direct sequence CDMA and wideband CDMA cellular networks,” *IEEE Commun. Mag.*, vol. 36, no. 9, pp. 48–54, 1998.

[5] L. Fukshansky and A. A. Shaar, “A new family of one-coincidence sets of sequences with dispersed elements for frequency hopping cdma systems.,” *Adv. Math. Comm.*, vol. 12, no. 1, pp. 181–188, 2018.

[6] D. Peng and P. Fan, “Lower bounds on the Hamming auto- and cross correlations of frequency-hopping sequences,” *IEEE Trans. Inf. Theory*, vol. 50, no. 9, pp. 2149–2154, 2004.

[7] O. A. Bamahdi and S. A. Zummo, “An Adaptive Frequency Hopping TechniqueWith Application to Bluetooth-WLAN Coexistence,” in *International Conference on Networking, International Conference on Systems and International Conference on Mobile Communications and Learning Technologies (ICNICONSMCL’06)*, 2006, p. 131.

[8] R. A. Poisel, *Information Warfare and Electronic Warfare Systems*. Artech House, 2013.

[9] R. A. Poisel, *Electronic Warfare Receivers and Receiving Systems*. Artech House, 2015.

[10] H. Fathallah, L. a. Rusch, and S. LaRochelle, "Passive Optical Fast Frequency-Hop CDMA Communications System," *J. Light. Technol.*, vol. 17, no. 3, pp. 397–405, 1999.

[11] Z. Zhou, X. Tang, D. Peng, and U. Parampalli, "New Constructions for Optimal Sets of Frequency-Hopping Sequences," *IEEE Trans. Inf. Theory*, vol. 57, no. 6, pp. 3831–3840, 2011.

[12] D. Marpaung, J. Yao, and J. Capmany, "Integrated microwave photonics," *Nat. Photonics*, vol. 13, no. 2, pp. 80–90, 2019.

[13] R. Kashyap, *Fiber Bragg Gratings*. Elsevier Science, 2009.

[14] X. Gu, A. F. Kockum, A. Miranowicz, Y. Liu, and F. Nori, "Microwave photonics with superconducting quantum circuits," *Phys. Rep.*, vol. 718–719, pp. 1–102, 2017.

[15] A. C. Torrezan, T. P. Mayer Alegre, and G. Medeiros-Ribeiro, "Microstrip resonators for electron paramagnetic resonance experiments," *Rev. Sci. Instrum.*, vol. 80, no. 7, p. 75111, Jul. 2009.

[16] M. Göppl *et al.*, "Coplanar waveguide resonators for circuit quantum electrodynamics," *J. Appl. Phys.*, vol. 104, no. 11, p. 113904, 2008.

[17] T.-T. Tsai *et al.*, "High throughput and label-free particle sensor based on microwave resonators," *Sensors Actuators A Phys.*, vol. 285, pp. 652–658, 2019.

[18] C. W. Zollitsch, J. O'Sullivan, O. Kennedy, G. Dold, and J. J. L. Morton, "Tuning high-Q superconducting resonators by magnetic field reorientation," *AIP Adv.*, vol. 9, no. 12, p. 125225, Dec. 2019.

[19] C. Triana, M. Varón, and D. Pastor, "Optical code division multiplexed fiber Bragg grating sensing networks," in *Proc.SPIE*, 2015, vol. 9634.

[20] A. Vanelli-Coralli *et al.*, "Chapter 10 - Cognitive radio scenarios for satellite communications: the CoRaSat project," S. Chatzinotas, B. Ottersten, and R. B. T.-C.

and C. S. S. De Gaudenzi, Eds. Academic Press, 2015, pp. 303–336.

[21] G. Kizer, “Digital Microwave Communication,” *Digital Microwave Communication*. 2013.

[22] E. Lopelli, J. van der Tang, and A. H. M. van Roermund, *Architectures and Synthesizers for Ultra-low Power Fast Frequency-Hopping WSN Radios*. Springer Netherlands, 2010.

[23] R. Corporation, “Rogers Corporation,” *RO4000 Series*, 2019. [Online]. Available: https://rogerscorp.com/advanced-connectivity-solutions/ro4000-series-laminates/ro4350b-laminates.

[24] C.-K. Lee, J. Kim, and S.-W. Seo, “Generation and performance analysis of frequency-hopping optical orthogonal codes with arbitrary time blank patterns,” in *IEEE International Conference on Communications*, 2001, vol. 4, pp. 1275–1279.

[25] T. C. and M. B. S. Edwards, *Foundations for microstrip circuit design*, 4th ed. Chichester, United Kingdom: IEEE Press Wiley, 2016.

[26] J. R. Kunz, Karl S.; Luebbers, *The Finite Difference Time Domain Method for Electromagnetics*, 1st Editio. CRC Press, 1993.

[27] A. Taflove and S. C. Hagness, *Computational Electrodynamics, the finite difference time domain method*, Third Edit. Norwood, MA: Artech House, 2005.

[28] A. Lempel and H. Greenberger, “Families of sequences with optimal Hamming-correlation properties,” *IEEE Transactions on Information Theory*, vol. 20, no. 1. pp. 90–94, 1974.

[29] E. S. Shivaleela, K. N. Sivarajan, and A. Selvarajan, “Design of a new family of two-dimensional codes for fiber-optic CDMA networks,” *J. Light. Technol.*, vol. 16, no. 4, pp. 501–508, 1998.

[30] J. Kim and C.-. Lee, “Generation and upper bound of one-coincidence sequences in frequency-hopping multiple-access systems,” *IEE Proc. - Commun.*, vol. 153, no. 5, pp. 740–745, 2006.

[31] R. Kashyap, “Chapter 4 - Theory of Fiber Bragg Gratings,” R. B. T.-F. B. G. (Second E. Kashyap, Ed. Boston: Academic Press, 2010, pp. 119–187.

[32] K. Drakakis, “A review of the available construction methods for Golomb rulers,” *Adv. Math. Commun.*, vol. 3, no. 3, pp. 235–250.

[33] G. E. Andrews and K. Eriksson, *Integer Partitions*. Cambridge University Press, 2004.

[34] W. C. Babcock, “Intermodulation Interference in Radio Systems,” *Bell Syst. Tech. J.*, vol. 32, no. 1, pp. 63–73, Jan. 1953.

[35] N. Memarsadeghi, “NASA Computational Case Study: Golomb Rulers and Their Applications,” *Comput. Sci. Eng.*, vol. 18, no. 6, pp. 58–62, 2016.

[36] C. Harpes and J. L. Massey, “Partitioning cryptanalysis BT - Fast Software Encryption,” 1997, pp. 13–27.

[37] W. Gautier, B. Schoenlinner, V. Ziegler, U. Prechtel, and W. Menzel, “High Q Micro-machined Cavity Resonator Filter in Low-Cost Silicon Technology,” in *2008 38th European Microwave Conference*, 2008, pp. 1193–1196.

[38] T. C. Edwards and M. B. Steer, “Loss and Power dependent Effects in Microstrip,” in *Foundations for Microstrip Circuit Design*, Wiley-IEEE Press, 2016, p. 688.

[39] D. M. Pozar, *Microwave Engineering, 4th Edition*. Wiley, 2011.

[40] K. C. Gupta, K. C. Gupta, R. Garg, I. J. Bahl, and P. Bhartia, *Microstrip Lines and Slotlines*. Artech House, 1996.

[41] C. K and L. Hsieh, “Analysis and Modeling of Ring Resonators,” in *Microwave Ring Circuits and Related Structures*, John Wiley & Sons, Ltd, 2005, pp. 5–54.

[42] R. Garg, I. Bahl, and M. Bozzi, *Microstrip Lines and Slotlines, Third Edition*. Artech House, 2013.

[43] M. B. Edwards, T. C. and Steer, “Microstrip Design at Low Frequencies,” in *Foundations for Microstrip Circuit Design*, John Wiley & Sons, Ltd, 2016, pp. 120–156.

[44] M. Krawczyk, “Microstrip resonators for circuit quantum electrodynamics,” Technische Universutat Munchen, 2011.

[45] I. C. Rodrigues, D. Bothner, and G. A. Steele, “Coupling microwave photons to a mechanical resonator using quantum interference,” *Nat. Commun.*, vol. 10, no. 1, p. 5359, 2019.

[46] M. V Schneider, “Microstrip lines for microwave integrated circuits,” *Bell Syst. Tech. J.*, vol. 48, no. 5, pp. 1421–1444, 1969.

[47] R. A. Pucel, D. J. Masse, and C. P. Hartwig, “Losses in Microstrip,” *IEEE Trans. Microw. Theory Tech.*, vol. 16, no. 6, pp. 342–350, 1968.

[48] N. H. L. Koster and R. H. Jansen, “The Equivalent Circuit of the Asymmetrical Series Gap in Microstrip and Suspended Substrate Lines,” *IEEE Trans. Microw. Theory Tech.*, vol. 30, no. 8, pp. 1273–1279, 1982.

[49] M. Kirschning, R. H. Jansen, and N. H. L. Koster, “Measurement and Computer-Aided Modeling of Microstrip Discontinuities by an Improved Resonator Method,” in *1983 IEEE MTT-S International Microwave Symposium Digest*, 1983, pp. 495–497.

[50] M. H. Zarifi, T. Thundat, and M. Daneshmand, “High resolution microwave microstrip resonator for sensing applications,” *Sensors Actuators A Phys.*, vol. 233, pp. 224–230, 2015.

[51] K. Yee, “Numerical solution of initial boundary value problems involving maxwell’s equations in isotropic media,” *IEEE Trans. Antennas Propag.*, vol. 14, no. 3, pp. 302–307, 1966.

[52] A. F. Oskooi, D. Roundy, M. Ibanescu, P. Bermel, J. D. Joannopoulos, and S. G. Johnson, “Meep: A flexible free-software package for electromagnetic simulations by the FDTD method,” *Comput. Phys. Commun.*, vol. 181, no. 3, pp. 687–702, 2010.

[53] U. S. Inan and R. A. Marshall, *Numerical Electromagnetics: The FDTD Method*. Cambridge University Press, 2011.

[54] W. Yu, *Electromagnetic Simulation Techniques Based on the FDTD Method*. Wiley, 2009.

[55] V. Teppati, A. Ferrero, and M. Sayed, *Modern RF and Microwave Measurement Techniques*. Cambridge University Press, 2013.

[56] "Appendix B: Characteristic Impedance, Delay Time, and Attenuation of Microstrips and Striplines," *Signal Integrity and Radiated Emission of High-Speed Digital Systems*. pp. 487–492, 14-Nov-2008.

[57] W. Yu, W. Li, A. Z. Elsherbeni, and Y. Rahmat-Samii, *Advanced Computational Electromagnetic Methods and Applications*. Artech House, 2015.

[58] H. R. Mohebbi, O. W. B. Benningshof, I. A. J. Taminiau, G. X. Miao, and D. G. Cory, "Composite arrays of superconducting microstrip line resonators," *J. Appl. Phys.*, vol. 115, no. 9, p. 94502, Mar. 2014.

[59] G. Vardulakis, S. Withington, D. J. Goldie, and D. M. Glowacka, "Superconducting kinetic inductance detectors for astrophysics," *Meas. Sci. Technol.*, vol. 19, no. 1, p. 15509, 2007.

[60] S. McHugh *et al.*, "A readout for large arrays of microwave kinetic inductance detectors," *Rev. Sci. Instrum.*, vol. 83, no. 4, p. 44702, Apr. 2012.

[61] T. Cecil *et al.*, "Kinetic Inductance Detectors for X-Ray Spectroscopy," *Phys. Procedia*, vol. 37, pp. 697–702, 2012.

[62] A. R. Hoskinson, C. Wu, and J. Hopwood, "Electrical modeling of strongly-coupled microstrip resonator arrays for microplasma generation," in *2011 Abstracts IEEE International Conference on Plasma Science*, 2011, p. 1.

[63] G. Wendin, "Quantum information processing with superconducting circuits: a review," *Reports Prog. Phys.*, vol. 80, no. 10, p. 106001, 2017.

[64] C. Yu *et al.*, "An impedance-modulated code-division microwave SQUID multiplexer," *Eng. Res. Express*, vol. 2, no. 1, p. 15011, 2020.

[65] M. Wegner *et al.*, "Microwave SQUID Multiplexing of Metallic Magnetic

Calorimeters: Status of Multiplexer Performance and Room-Temperature Readout Electronics Development," *J. Low Temp. Phys.*, vol. 193, no. 3, pp. 462–475, 2018.

[66] Y. H. Wu, Y. C. Kuan, and M. C. F. Chang, "Interference-tolerant multi-user radar system using one-coincidence frequency hopping code with 1GHz bandwidth at 24GHz," in *2016 IEEE MTT-S International Microwave Symposium (IMS)*, 2016, pp. 1–4.